conveniently purified by Ni-NTA chromatography. The affinity-purified TB-spacer and the TB-Z appeared on SDS-PAGE as protein bands with molecular masses of approximately 10 kDa and 12 kDa, respectively (Fig. 1b, CBB). Since the molecular masses predicted from the primary structures of the TB-spacer and TB-Z were 9.2 kDa and 14.9 kDa, respectively, the bands we observed presumably represented their monomers. In contrast, protein bands that were predicted tetramers of the TB-spacer and TB-Z were observed by native PAGE (Fig. 1c, left). In addition, size exclusion chromatography of the TB-Z showed a single chromatographic peak with an estimated molecular mass of 74.8 kDa (Fig. 1c, right), which appeared substantially higher than its calculated mass (i.e., 59.6 kDa for the tetramer). This discrepancy may be attributed to the long rod-like structure of the TB coiled-coil domain, because such molecules generally appear higher in molecular mass than globular proteins of the same mass. These results indicated that the TB-based constructs were secreted from recombinant *E. coli* predominantly as tetramers but were disassembled into monomers in the presence of SDS. The TB-Z, but not the TB-spacer, was shown to bind to the Ig molecule (Fig. 1b, WB).

Next, Cys residues were introduced into the wild-type sequence of the TB-Z for use as a specific antigen-coupling site, because no Cys residues existed within the TB and Z protein moieties. Three candidate sites were selected for Cys insertion. Two of these sites represented Ser substitutions (Ser3 and Ser52), which were chosen out of the four possible Ser residues (Ser3, Ser26, Ser47, and Ser52) because of their presumed degree of side chain exposure to the surface of the coiled-coil domain, based on the 3-dimensional (3D) crystal structure (PDB accession no. 1YBK), and one site represented *de novo* Cys insertion based on the presumed molecular flexibility within the spacer region. Thus, three TB-Z constructs containing Cys residues [TB(Cys)-Z] were engineered: TB(S3C)-Z, TB(S52C)-Z, and TB(C60)-Z. The TB(S3C)-Z construct failed to be expressed in any cellular compartment or in the culture supernatant, but the TB(S52C)-Z and TB(C60)-Z constructs (Fig. 1a, region b) were fully expressed in the culture supernatant, as observed for parental TB-Z, and were purified by Ni-NTA chromatography. For the affinity-purified TB(Cys)-Z [TB(S52C)-Z and TB(C60)-Z], but not for the TB-Z, dimers were observed as predominant molecular species by SDS-PAGE analysis (Fig. 1d, compare lanes 1 with lanes 2 and 3), indicating that disulfide bonds formed between the two subunit pairs within the tetramer. The TB(Cys)-Z could also bind to the Ig molecule, as seen for the TB-Z (Fig. 1d, WB).

COMP-based constructs, i.e., the COMP, COMP-spacer, and COMP-Z, were also engineered (Fig. 2a) and analyzed for their expression in *E. coli*. All three constructs were expressed in culture supernatants similarly to the TB-based constructs. They were purified by Ni-NTA chromatography and were subjected to SDS-PAGE and native PAGE (Fig. 2b and c). Unlike the TB-based proteins, the COMP-based proteins appeared as several bands of various molecular masses under denaturing conditions (Fig. 2b). However, by native PAGE, they appeared predominantly as pentameric forms (Fig. 2c, left). Only the COMP-Z bound to the Ig molecule (Fig. 2b and c, WB). A single chromatographic peak was observed for the COMP-Z by size exclusion chromatography (Fig. 2c, right); its estimated

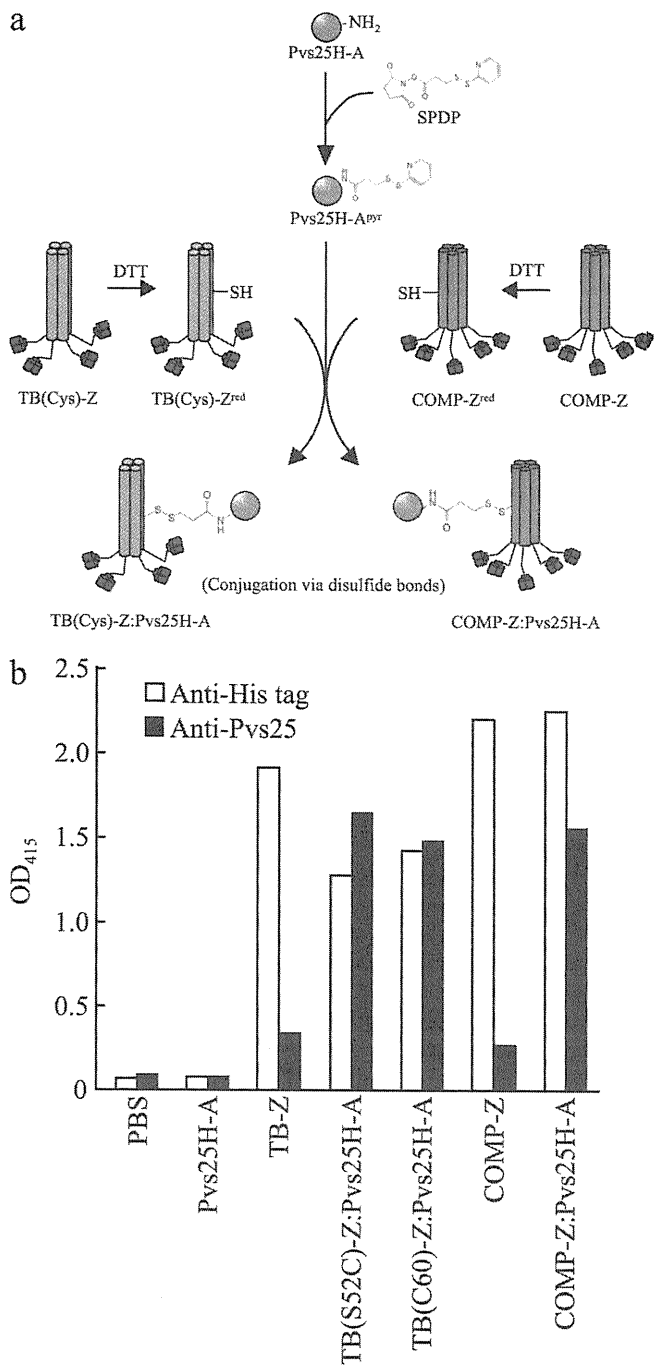

FIG. 3. Chemical conjugation of Pvs25H-A to TB(Cys)-Z [TB(S52C)-Z or TB(C60)-Z] or COMP-Z. (a) Chemical conjugation scheme for the construction of the TB(Cys)-Z:Pvs25H-A and COMP-Z:Pvs25H-A tricomponent complexes. The heterobifunctional cross-linker *N*-succinimidyl-3-(2-pyridyldithio)propionate (SPDP) was used to link the Pvs25H-A antigen (22) to the TB(Cys)-Z or COMP-Z delivery molecule via disulfide bonds. The delivery molecules were first treated with dithiothreitol (DTT) to expose free sulfhydryls [designated TB(Cys)-Z^{red} or COMP-Z^{red}], and then pyridyldithiol-activated Pvs25H-A (Pvs25H-A^{pyr}) was reacted with the delivery molecules to generate the tricomponent complexes. (b) The complexes generated were analyzed by a human IgG-ELISA using an anti-His (open bars) or anti-Pvs25 (filled bars) antiserum.

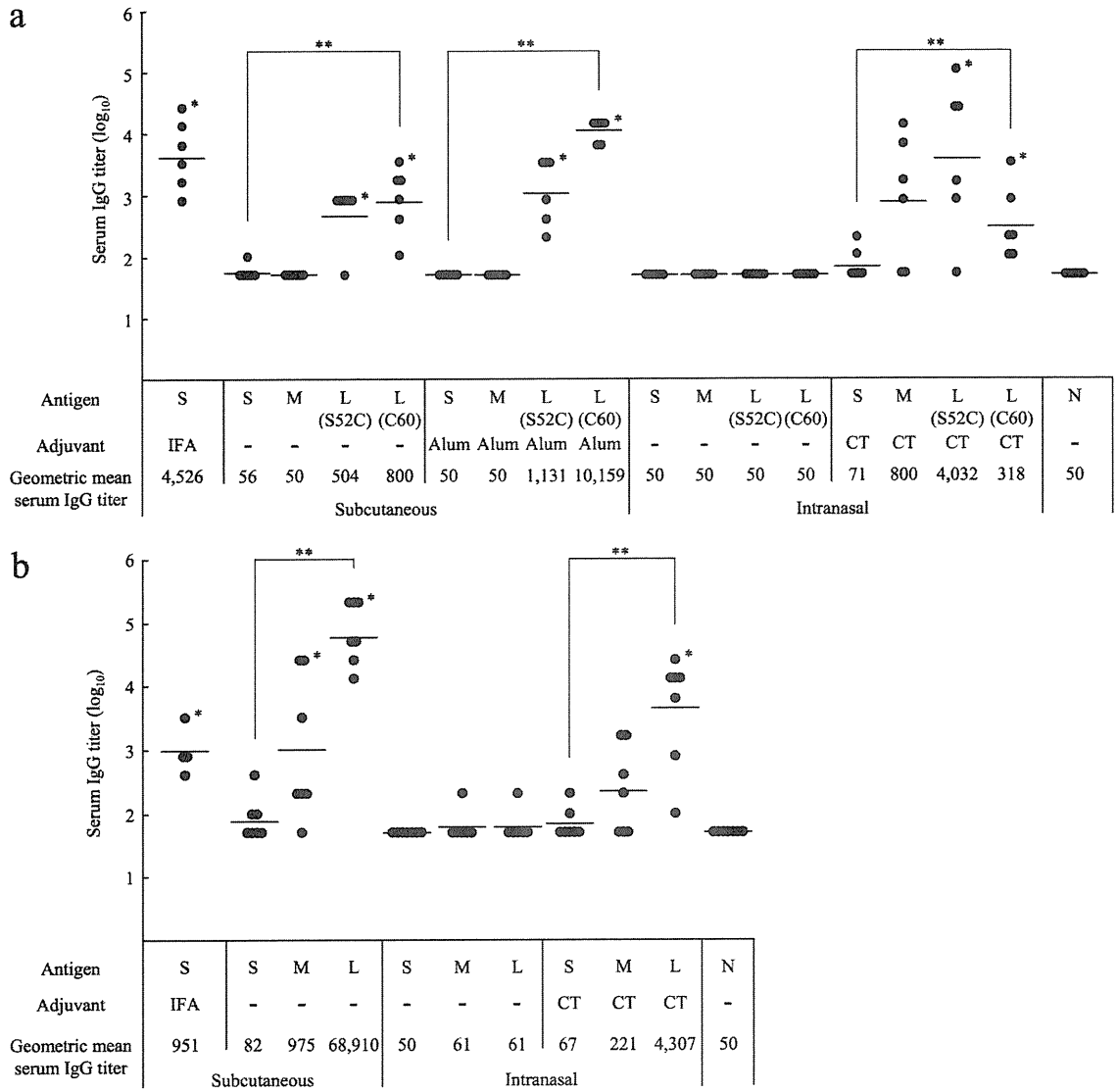

FIG. 4. Immunogenicity of the tricomponent complex. Mice were immunized by the subcutaneous or intranasal route three times, at weeks 0, 2, and 4, and antisera were collected 2 weeks after the third immunization to evaluate the Pvs25-specific IgG titers. All mice received 30 μg of the Pvs25H-A antigen as a conjugated or unconjugated protein. Incomplete Freund's adjuvant (IFA), aluminum hydroxide (Alum), or cholera toxin (CT) (1 μg) was used as the subcutaneous or intranasal adjuvant, as indicated. N, nonimmune sera from unimmunized control mice. Antibody titers were defined either as the serum dilution that resulted in an OD_{415} of 0.1 or as the serum dilution for which a 1-point-higher dilution (2-fold) resulted in an OD_{415} of <0.1. (a) Female BALB/c mice (six per group) were immunized with either the Pvs25H-A antigen alone (30 μg) (S), a mixture of the antigen (30 μg) and the TB-Z (21.4 μg) (M), the TB(S52C)-Z:Pvs25H-A tricomponent complex (51.4 μg) [L(S52C)], or the TB(C60)-Z:Pvs25H-A tricomponent complex (51.4 μg) [L(C60)]. (b) Female BALB/c mice (four or seven per group) were immunized with either the Pvs25H-A antigen alone (30 μg) (S), a mixture of the antigen (30 μg) and the COMP-Z (10.8 μg) (M), or the COMP-Z:Pvs25H-A tricomponent complex (40.8 μg) (L). Asterisks indicate significant differences from the unimmunized control group by the Wilcoxon-Mann-Whitney test (*, $P < 0.05$) or among the three groups indicated [S, M, and L(S52C) or L(C60) for the TB-based constructs, or S, M, and L for the COMP-based constructs] by the Kruskal-Wallis test (**, $P < 0.001$).

molecular mass was 79.8 kDa, higher than its calculated mass (i.e., 72.5 kDa for the pentamer). This difference may be attributed to the rod-like structure of the COMP coiled-coil domain, as observed for the TB-Z.

Taking these findings together, we concluded that the TB-Z and COMP-Z were secreted as tetrameric and pentameric forms, respectively, retaining their binding affinities for the Ig molecule. Their expression levels reached 30 mg/liter of bacterial culture. Multimerization of the Z domain mediated by the coiled-coil domain assembly significantly enhanced the avidity of the delivery molecules for the Ig molecule, as evidenced by the fact that the disassembled monomeric Z domain exhibited reduced affinity for the Ig molecule (Fig. 1d and 2b). This was also true when the Z domain was expressed as a single independent monomeric protein (data not shown).

Chemical conjugation of the Pvs25H-A antigen to the TB(Cys)-Z or COMP-Z delivery molecule to generate tricomponent complexes. The TB(Cys)-Z [TB(S52C)-Z and TB(C60)-Z] or COMP-Z constructs contained one artificially introduced (Fig. 1a, region b) or two inherent (Fig. 2a, region

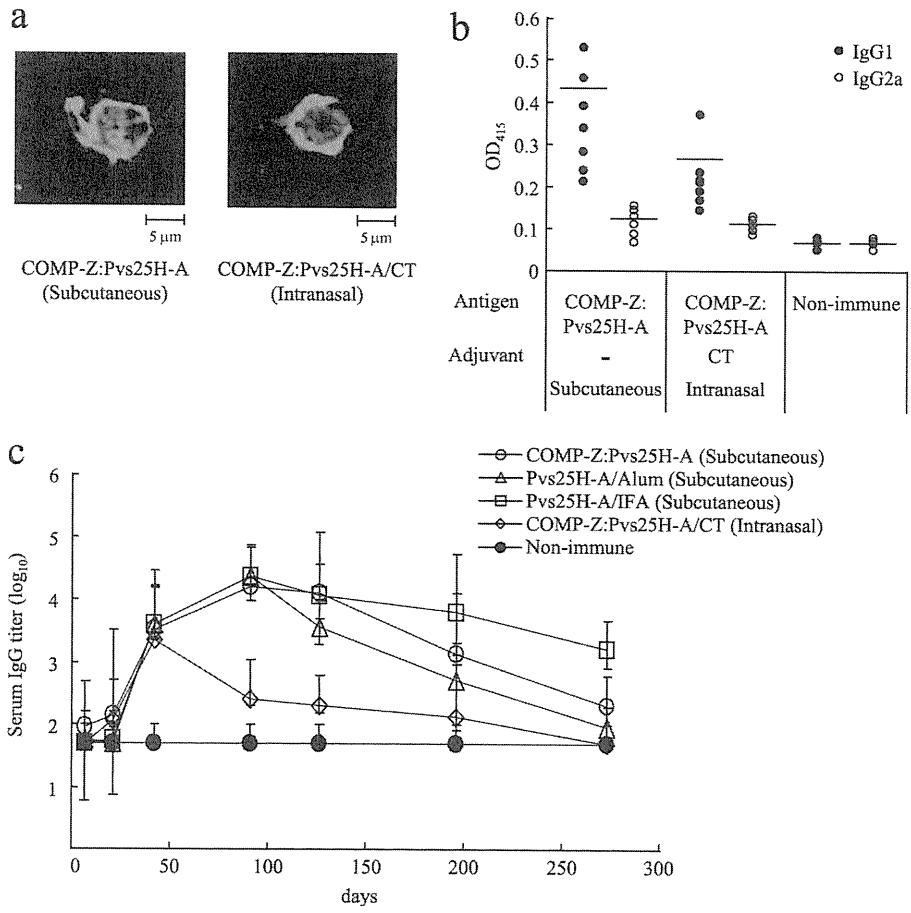

FIG. 5. Parasite recognition, IgG subclasses, and maintenance of the antisera induced by the COMP-Z-based tricomponent complex. The antisera obtained from the immunized mice in the experiments described in the legend to Fig. 4 were analyzed for parasite recognition (a) and IgG subclasses (b). (a) The ookinete-specific reactivities of the antisera induced by subcutaneous or intranasal immunization with the COMP-Z:Pvs25H-A tricomponent complex were determined by immunofluorescence analysis. The antisera specifically recognized native Pvs25 protein expressed on the surfaces of immature *Plasmodium vivax* ookinetes. (b) Pvs25H-A-specific IgG1 and IgG2a analysis of the antisera induced by the COMP-Z:Pvs25H-A tricomponent complex. (c) Mice were immunized as described in the legend to Fig. 4, and the Pvs25H-A-specific serum IgG responses over a prolonged period were evaluated. Antibody titers were defined as described in the legend to Fig. 4.

b) Cys residues per subunit, respectively. The recombinant Pvs25H-A protein expressed in the yeast *Pichia pastoris* (22) was chemically conjugated to the delivery molecules via the sulfhydryl groups of the Cys residues by a heterobifunctional cross-linker, SPDP (Fig. 3a). Since disulfide bonds in the Pvs25 protein are known to be important for vaccine function (16, 31, 32), the delivery molecules, but not the Pvs25H-A antigen, were treated with a reducing agent to expose free sulfhydryls, making them reactive with the pyridyldithiol groups added to Pvs25H-A (Fig. 3a). The human IgG-ELISA indicated that all complexes, but not the delivery molecules alone, reacted strongly with an anti-Pvs25 antiserum (Fig. 3b). In contrast, all proteins, except for Pvs25H-A, which could not be captured by the human IgG, reacted to the anti-His antibody, since each of them contained a hexahistidine (6×His) tag (Fig. 3b). These results indicated that delivery molecules that retained affinity for the Ig molecule were loaded with the Pvs25H-A antigen to generate the tricomponent complexes.

Immunogenicity of the tricomponent complexes. Female BALB/c mice (4 to 7 per group) were immunized with the Pvs25H-A antigen alone (designated S), a mixture of the antigen and the delivery molecules (designated M), or the antigen ligated to the delivery molecules (the tricomponent complexes, designated L), by the s.c. or i.n. route, with or without the indicated adjuvants, at weeks 0, 2, and 4, and antisera collected at week 6 were analyzed for the antigen-specific IgG (Fig. 4a and b [TB-based and COMP-based proteins, respectively]). We found that for s.c. immunization, (i) the tricomponent complexes consistently induced higher IgG responses than the antigen alone or the mixture of proteins, regardless of the adjuvant present; (ii) the mixture of the antigen with the COMP-Z, but not with the TB-Z, augmented the response; (iii) the COMP-based tricomponent complex induced higher responses than the TB-based tricomponent complexes; (iv) the COMP-based tricomponent complex without the addition of an extraneous adjuvant induced a greater response than that induced by the antigen emulsified with IFA. We also found that for i.n. immunization, the general trends were similar to those observed for s.c. immunization, but supplementation with CT was essential for induction of the response. We tested the i.p. and intravenous immunization routes and found no immune-enhancing effects (data not shown).

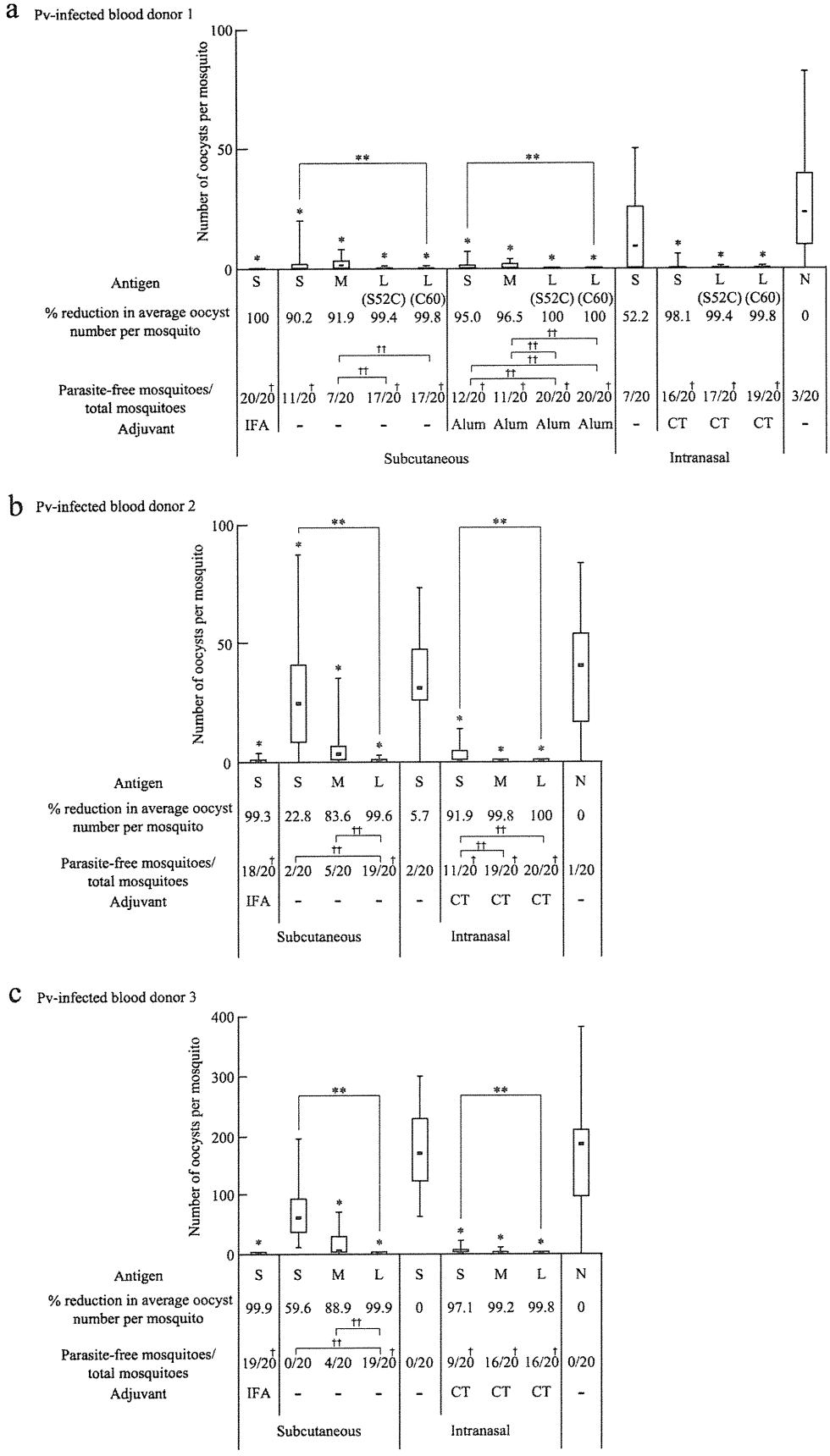
a Pv-infected blood donor 1
Number of oocysts per mosquito
100
50
0
**
**
Antigen
S S M L L S M L L S S L L N
(S52C) (C60) (S52C) (C60) (S52C) (C60)
% reduction in average oocyst number per mosquito
100 90.2 91.9 99.4 99.8 95.0 96.5 100 100 52.2 98.1 99.4 99.8 0
Parasite-free mosquitoes/ total mosquitoes
20/20† 11/20† 7/20 17/20† 17/20† 12/20† 11/20† 20/20† 20/20† 7/20 16/20† 17/20† 19/20† 3/20
Adjuvant
IFA - - - - Alum Alum Alum Alum - CT CT CT -
Subcutaneous
Intranasal
b Pv-infected blood donor 2
Number of oocysts per mosquito
100
50
0
**
**
Antigen
S S M L S S M L N
% reduction in average oocyst number per mosquito
99.3 22.8 83.6 99.6 5.7 91.9 99.8 100 0
Parasite-free mosquitoes/ total mosquitoes
18/20† 2/20 5/20 19/20† 2/20 11/20† 19/20† 20/20† 1/20
Adjuvant
IFA - - - - CT CT CT -
Subcutaneous
Intranasal
c Pv-infected blood donor 3
Number of oocysts per mosquito
400
300
200
100
0
**
**
Antigen
S S M L S S M L N
% reduction in average oocyst number per mosquito
99.9 59.6 88.9 99.9 0 97.1 99.2 99.8 0
Parasite-free mosquitoes/ total mosquitoes
19/20† 0/20 4/20 19/20† 0/20 9/20† 16/20† 16/20† 0/20
Adjuvant
IFA - - - - CT CT CT -
Subcutaneous
Intranasal

Parasite recognition, IgG subclasses, and the maintenance of induced serum IgG levels by the COMP-Z-based tricomponent complex. The antisera obtained from the immunized mice as described for Fig. 4 were analyzed for parasite recognition and IgG subclasses. The antisera specifically recognized the surfaces of immature *P. vivax* ookinetes as determined by immunofluorescence (Fig. 5a). The antisera predominantly contained the IgG1 subclass, indicative of a Th2 response (Fig. 5b). In a separate experiment, mice were immunized as described for Fig. 4, and the Pvs25H-A-specific serum IgG responses over a prolonged period were evaluated (Fig. 5c). The IgG titers attained by s.c. immunization with the tricomponent complex were comparable to those attained by the IFA- or Alum-assisted immunization regimen up to day 100. However, after this time point, the tricomponent complex-induced response decreased below the level of the IFA-assisted response but remained higher than the Alum-assisted response. In contrast, the period of tricomponent complex-induced serum IgG maintenance was significantly shorter via the i.n. immunization route than via the s.c. route.

TBV efficacies of the tricomponent complexes. The antisera obtained from the immunized mice as described for Fig. 4 were evaluated for their transmission-blocking vaccine (TBV) efficacies against *P. vivax* parasites by a membrane feed assay using *P. vivax*-infected blood samples obtained from *P. vivax* patients in Thailand. The experiments were performed in triplicate, once with the TB-based (Fig. 6a) and twice with the COMP-based (Fig. 6b and c) tricomponent complex-induced mouse antisera, using blood samples from three volunteer donors. The experiments with blood samples from *P. vivax*-infected donors 1 and 2 demonstrated similar levels of infection, whereas the experiment with a blood sample from donor 3 showed a much greater level of infection.

In all of the blood samples, the average number of oocysts per mosquito was reduced by more than 99% from that with nonimmune control serum (N) when the mouse antisera induced by s.c. immunization with the Pvs25H-A antigen alone (S) emulsified with IFA were mixed with the patient's blood samples. Omission of the adjuvant significantly abated the effect (20 to 90% reduction) (Fig. 6a to c). However, loading of the antigen onto the delivery molecules (L) resulted in a dramatic restoration of vaccine efficacy, increasing it to close to 100% (Fig. 6a to c). Loading of the antigen onto the TB-based delivery molecules resulted in a higher vaccine efficacy than that for the antigen alone mixed with Alum (Fig. 6a), and the use of Alum further increased the efficacy of the tricomponent complexes, conferring complete parasite transmission blockade [Fig. 6a, L(S52C) with Alum and L(C60) with Alum]. The two TB-based tricomponent complexes were equally effective (Fig. 6a). For the i.n. immunization, the vaccine efficacy of the antigen alone mixed with CT was high, conferring a >90% reduction, and loading of the antigen onto the delivery molecules further increased the efficacy (Fig. 6a to c). The mixture of the antigen and delivery molecules (M) enhanced vaccine efficacy over that of the antigen alone, and this was particularly notable for the COMP-Z (Fig. 6b and c). These results were consistent with those obtained for the Pvs25H-A antigen-specific serum IgG titers (Fig. 4).

In the blood sample from donor 3 (Fig. 6c), the level of *P. vivax* infection was much higher than that in the other two samples (Fig. 6a and b). Despite this, the COMP-Z-based tricomponent complex conferred a robust transmission blockade even without Alum, and this efficacy was as high as the efficacy achieved by administering the antigen with IFA (Fig. 6c). Taking these findings together, we concluded that the Pvs25H-A antigen, when loaded onto a TB(Cys)-Z or COMP-Z delivery molecule, was transformed into a robustly efficacious TBV.

Essentiality of each component of the tricomponent complex and effects of the ligand arrangement on the immune response. To determine if there were any dispensable components of the tricomponent complex, we compared the immunogenicities of various combinations of the three components. We found, for both the s.c. and i.n. immunization routes, that all three components were essential and were required to be concomitantly integrated into the fusion complex for efficient induction of the immune response (Fig. 7a). As expected, a dicomponent molecule (i.e., a mixture of two physically separate components, such as the antigen plus the core motif or the antigen plus the ligand) failed to induce any response (data not shown). These results indicated that not only were all three components indispensable; they also needed to be integrated into the fusion complex.

Next, to evaluate whether a unique molecular configuration of the tricomponent complex is important for its immunopotentiating activity, we compared the immunogenicity of the COMP-Z:Pvs25H-A tricomponent complex with that of a fusion complex in which five tandemly repeated Z domains were chemically fused to the antigen (ZV:Pvs25H-A). For the construction of the ZV:Pvs25H-A fusion complex, chemical conjugation was conducted by reacting a free sulfhydryl group of the C-terminally introduced Cys residue in the ZV delivery

FIG. 6. TBV efficacies of the tricomponent complexes. The antisera (i.e., 1/2 dilution of the pooled antisera) obtained from the immunized mice in the experiments described in the legend to Fig. 4 were analyzed for TBV efficacy. The data are expressed as median numbers of oocysts per mosquito (bars within boxes), with 25% and 75% quartiles (the boxes) and ranges (whiskers above and below boxes). The percentage of reduction was defined as the reduction in the average number of oocysts for each group from that for the unimmunized control group. The number of parasite-free mosquitoes compared with the total number of mosquitoes (20 mosquitoes) is also provided. Experiments were performed three times using different blood samples from three donors. A *Plasmodium vivax*-infected blood sample from donor 1 (a) was used to evaluate the TBV efficacies of the TB-based constructs, and *P. vivax*-infected blood samples from donors 2 and 3 (b and c) were used for the COMP-based constructs. Asterisks and daggers indicate significant differences from the unimmunized control group by the Wilcoxon-Mann-Whitney test (*, $P < 0.001$), among the three groups indicated [S, M, and L(S52C) or L(C60) for the TB-based constructs, or S, M, and L for the COMP-based constructs] by the Kruskal-Wallis test (**, $P < 0.001$), from the unimmunized control group by the χ^2 test (†, $P < 0.005$), and between the two groups indicated by the χ^2 test (††, $P < 0.005$). The data for 10 immunization groups (8 S groups and 2 N groups) analyzed using blood samples from donors 2 and 3 were the same as those derived from a previously published study (22).

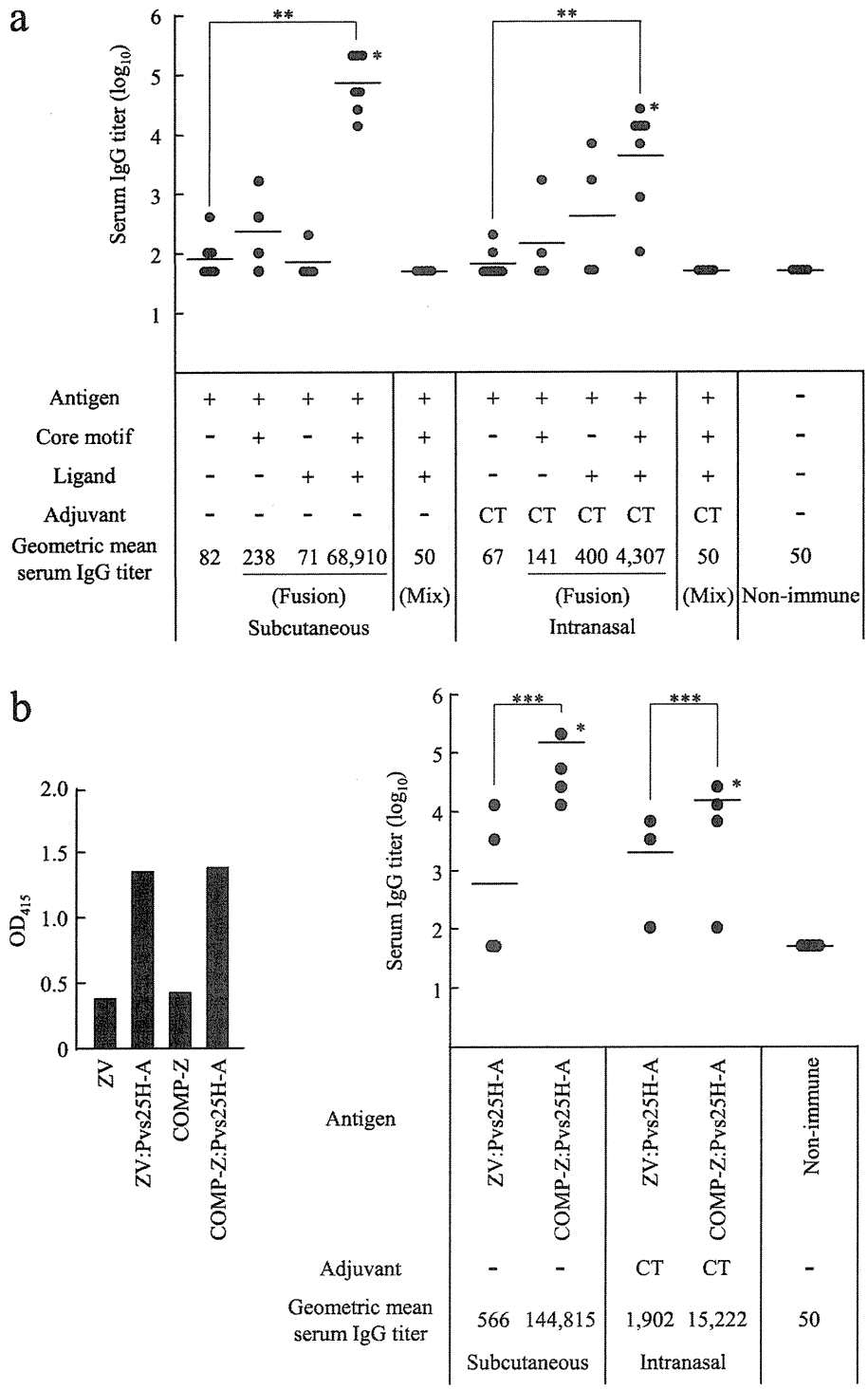

FIG. 7. Essentiality of each component of the tricomponent complex and effects of the ligand arrangement on the immune response. Mice were immunized by the subcutaneous or intranasal route three times, at weeks 0, 2, and 4, and antisera were collected 2 weeks after the third immunization in order to evaluate the Pvs25-specific IgG titers. All mice received 30 μg of the Pvs25H-A antigen as a conjugated or unconjugated protein. Cholera toxin (CT) (1 μg) was used as the intranasal adjuvant. Antibody titers were defined as described in the legend to Fig. 4. Asterisks indicate significant differences from the unimmunized control group by the Wilcoxon-Mann-Whitney test (*, $P < 0.05$), among the four groups indicated by the Kruskal-Wallis test (**, $P < 0.001$), or between the two groups indicated by the Wilcoxon-Mann-Whitney test (***, $P < 0.01$). (a) Female BALB/c mice (seven or four per group) were immunized with one of the following, from left to right: the Pvs25H-A antigen alone (30 μg), the COMP-spacer:Pvs25H-A fusion complex (36.3 μg), the antigen fused directly to the monomeric Z domain (34.5 μg), the COMP-Z:Pvs25H-A tricomponent complex (40.8 μg), or a mixture of the antigen (30 μg), the COMP-spacer (6.3 μg), and the Z domain (4.5 μg). The data for four groups (the antigen alone, the antigen mixed with CT, and the tricomponent complex administered by the s.c. or i.n. route) are duplicates of the data presented in Fig. 4b. (b) Female BALB/c mice (seven or four per group) were immunized with the ZV:Pvs25H-A fusion complex (43.2 μg) or the COMP-Z:Pvs25H-A tricomponent complex (40.8 μg). The ZV:Pvs25H-A fusion complex was generated by reacting a free sulfhydryl group of the C-terminally introduced Cys residue in the ZV delivery molecule, which consists of five tandemly repeated Z domains, with the SPDP-modified Pvs25H-A antigen. Chemical conjugation between the antigen and the ZV delivery molecule was confirmed by a human IgG-ELISA using an anti-Pvs25 antiserum (left) prior to immunization experiments (right).

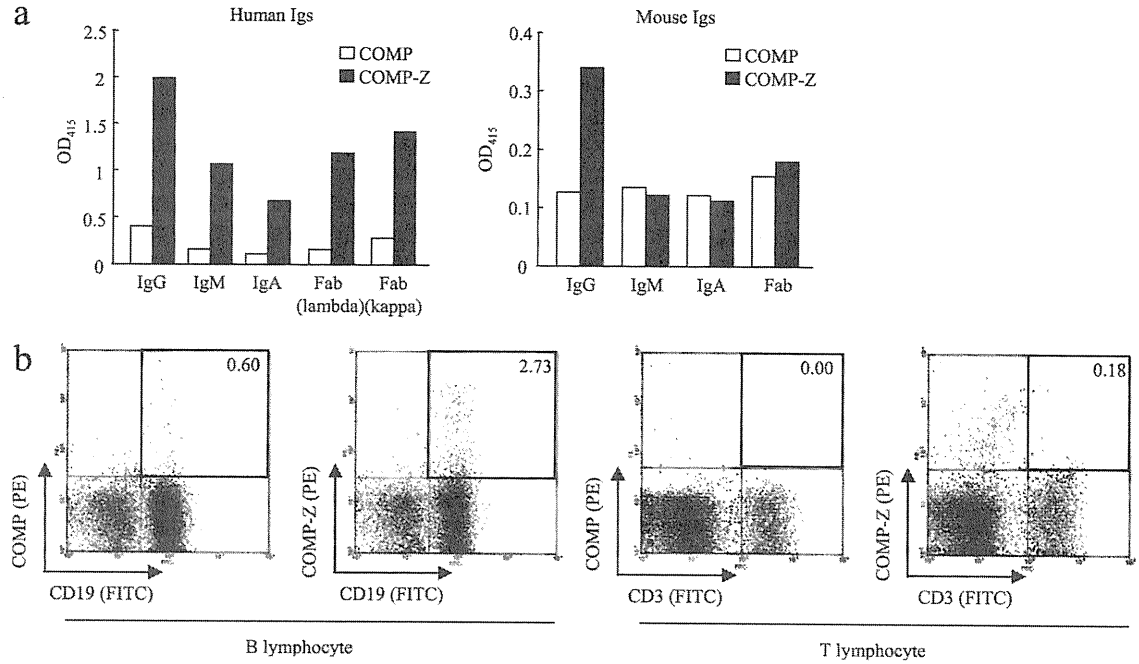

FIG. 8. Analysis of the target cells of the tricomponent complex. (a) Affinity of the COMP-Z (filled bars) for various human or mouse immunoglobulin (Ig) isotypes. The COMP coiled-coil domain devoid of the Z domain ligand (open bars) was used as a negative control. (b) Flow cytometry of the COMP-Z. Freshly isolated splenocytes were first double stained with an FITC-conjugated anti-CD19 or anti-CD3 antibody and with PE-conjugated COMP or COMP-Z and were then analyzed on a FACSCalibur flow cytometer.

molecule with the SPDP-modified Pvs25H-A antigen. Chemical conjugation between the antigen and ZV was found to be as efficient as conjugation between the antigen and COMP-Z, as determined by a human IgG-ELISA (Fig. 7b, left). Although the ZV-based fusion complex induced a higher serum IgG response than the antigen alone or the antigen fused to a single or two tandemly repeated Z domains (data not shown), it was much less efficacious than the tricomponent complex (Fig. b, right). This suggested that multiple ligands in a parallel arrangement, such as that found in the tricomponent complex, represent a better molecular configuration than the same ligands with the same valence, arranged in a tandemly repeated fashion, like those found in the ZV fusion complex.

Analysis of the target cells of the tricomponent complex. In our first attempt to elucidate the mechanism behind the immune-enhancing effect of the tricomponent complex, the profiles of the binding of COMP-Z to various human or mouse Ig isotypes were analyzed (Fig. 8a). The affinity for human IgG was the highest, but the molecule also bound to human IgM, IgA, and even Fab molecules. In addition, the COMP-Z bound to mouse IgG but not to mouse IgM, IgA, or Fab. We found that the COMP-Z exhibited higher affinity for human IgG than for mouse IgG.

We hypothesized that the most likely target of the COMP-Z *in vivo* is B lymphocytes, since they harbor surface Ig receptors of various isotypes. Fluorescence-activated cell sorter (FACS) analysis of a fluorescein-conjugated COMP-Z indicated that it bound to $CD19^+$ B lymphocytes but not to $CD3^+$ T lymphocytes *in vitro* (Fig. 8b). However, the COMP-Z did not bind to other immune cell types, including $CD11c^+$ MHC class II^+ DCs, $CD11b^+$ macrophages, and $CD11b^+$ $Gr\text{-}1^+$ neutrophils, in this assay (data not shown). These data suggested that the immune-enhancing effect of the tricomponent complex is based partially, if not exclusively, on its B lymphocyte-targeting capability. The most likely reasons why only a small fraction of $CD19^+$ mouse B lymphocytes bound to the COMP-Z (Fig. 8b, second panel from the left) were that the delivery molecule exhibited a lower affinity for mouse IgG than for human IgG and that the molecule did not efficiently bind to other mouse Ig isotypes.

Protective efficacy of the tricomponent complex against a lethal malaria parasite infection in mice. Finally, we evaluated whether the tricomponent complex is effective at inducing protective immunity against a lethal malaria parasite infection. The MSP1-19 fragment of the rodent malaria *P. yoelii* was expressed and purified from *P. pastoris* by Ni-NTA chromatography, followed by size exclusion chromatography to obtain a properly folded antigen (T. Harakuni et al., submitted for publication). Then the purified MSP1-19 antigen was loaded onto the TB(S52C)-Z or COMP-Z delivery molecule by the same chemical coupling method used for the Pvs25H-A antigen, as schematized in Fig. 3a. Successful coupling of MSP1-19 to the delivery molecules was confirmed by the human IgG-ELISA (Fig. 9a).

Female C57BL/6 mice (10 per group) were s.c. administered either the MSP1-19 antigen mixed with IFA or Alum or the TB(S52C)-Z:MSP1-19 or COMP-Z:MSP1-19 tricomponent complex mixed with Alum, three times, at weeks 0, 2, and 4. A strong serum IgG response was observed for MSP1-19 with IFA, followed by the TB- and COMP-based tricomponent complexes; the weakest response was observed with the MSP1-19–Alum immunization regimen (Fig. 9b). At week 6, mice were challenged i.p. with a lethal number of parasitized erythrocytes (1×10^4 *P. yoelii* 17XL-parasitized RBCs/mouse), and

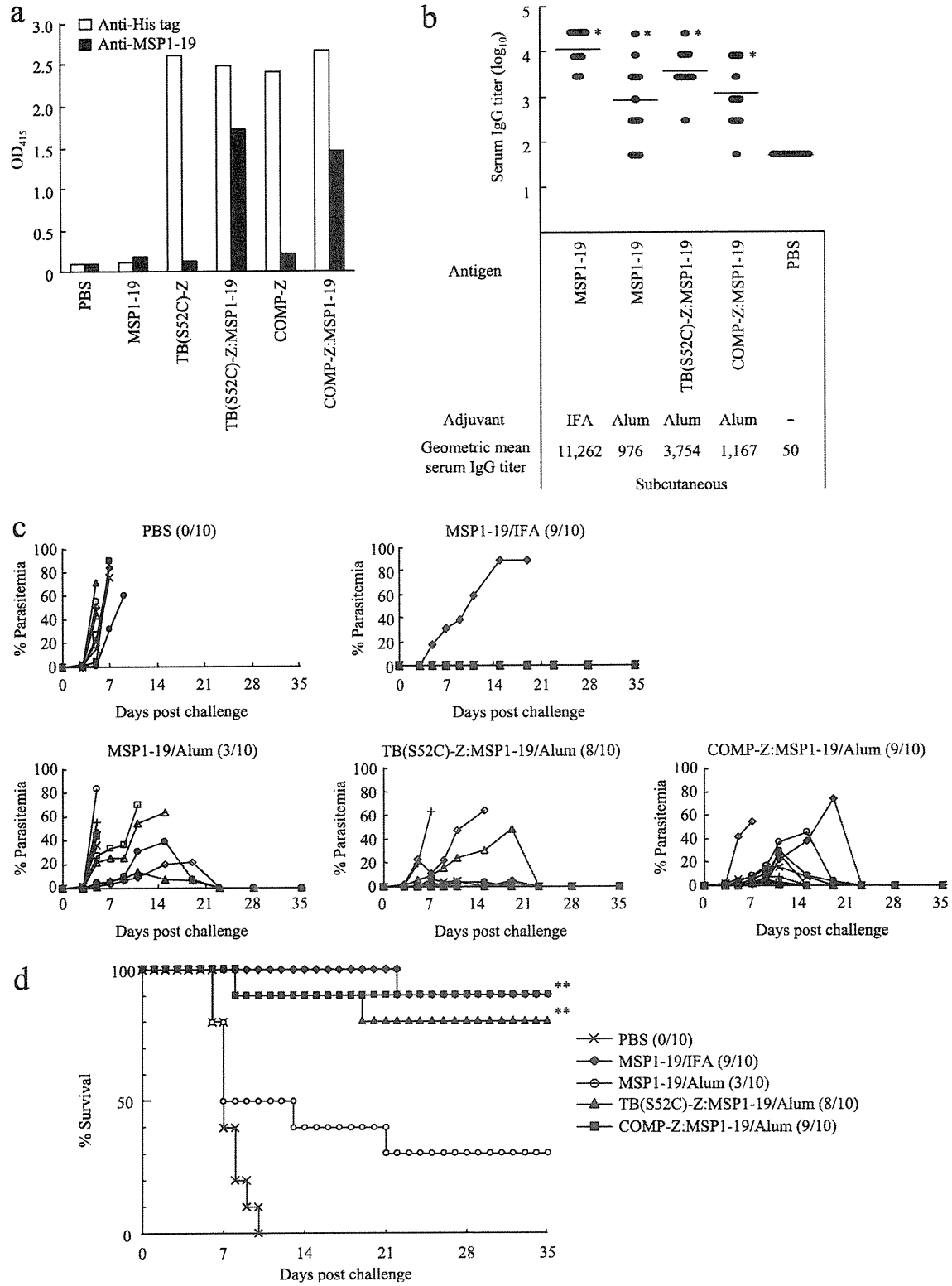

FIG. 9. Protective efficacy of the tricomponent complex against a lethal malaria parasite infection in mice. (a) The TB(S52C)-Z:MSP1-19 or COMP-Z:MSP1-19 tricomponent complex was generated by the same chemical coupling method used for the Pvs25H-A antigen, as schematized in Fig. 3a. The complexes generated were analyzed by a human IgG-ELISA using an anti-His (open bars) or anti-MSP1-19 (filled bars) antiserum. (b to d) Female C57BL/6 mice (10 per group) were immunized with the MSP1-19 antigen alone (30 μg), the TB(S52C)-Z:MSP1-19 tricomponent complex (51.4 μg), or the COMP-Z:MSP1-19 tricomponent complex (40.8 μg) by the subcutaneous route, three times, at weeks 0, 2, and 4. All mice received 30 μg of the MSP1-19 antigen as a conjugated or unconjugated protein. Incomplete Freund's adjuvant (IFA) or aluminum hydroxide (Alum) was used as the adjuvant. Antibody titers were defined as described in the legend to Fig. 4. Immunized mice were challenged 2 weeks after the third immunization with a lethal number of *Plasmodium yoelii* 17XL-parasitized erythrocytes (1×10^4 infected red blood cells/mouse) by the intraperitoneal route. Serum IgG titers immediately before parasite challenge (b), levels of parasitemia (c), and survival rates (d) are shown. In panels c and d, the number of mice who survived among the 10 mice in each group is given in parentheses. Asterisks indicate significant differences ($P < 0.001$) from the PBS control group by the Wilcoxon-Mann-Whitney test (*) or the log rank test (**).

then parasitemia was monitored for 5 weeks (Fig. 9c). All mice administered PBS died within 10 days postchallenge (Fig. 9d). In contrast, mice immunized with the tricomponent complex showed an 80 to 90% survival rate, and mice immunized with MSP1-19–IFA or MSP1-19–Alum showed a 90% or 30% survival rate, respectively, indicating that loading of the antigen onto the delivery molecules significantly augmented protective efficacy against lethal parasite infection.

Taken together, the results obtained from the transmission-blocking experiments (Fig. 6) and the rodent malaria infection experiments (Fig. 9) demonstrated that the tricomponent complexes not only induce antibodies that possess strong parasite-killing activity in the mosquito midgut but also provide substantial protective immunity against parasite replication in the infected mammalian host.

DISCUSSION

Recombinant protein-based anti-infectious subunit vaccines are attractive alternatives to conventional vaccines produced by inactivation or attenuation of pathogenic organisms, because they are likely to be safer to produce and administer. Furthermore, vaccines against some pathogens, such as malaria parasites and other parasitic microbes, can be produced only by recombinant techniques, because they defy conventional methods of vaccine production. However, nonreplicating, inert recombinant antigens are often weakly immunogenic, and therefore, adjuvants (i.e., immune-enhancing materials that physiologically activate immune cells and/or delivery systems that increase the concentration of antigens near or at APCs in lymphoid organs, such as lymph nodes) are indispensable components of such vaccines (2, 25, 27). Therefore, the fact that recombinant protein antigens are often weak immunogens does not nullify their potential as good vaccines, with adjuvants playing an essential role in enhancing the immunogenicity of such weakly immunogenic antigens.

In this study, we reported a novel antigen delivery system that was able to target B lymphocytes by exploiting the α-helical coiled-coil domain-mediated multimerized IBDs as target ligands. Of the various immune cells, DCs are generally considered the most efficient APCs, but the antigen-presenting ability of B lymphocytes has recently attracted renewed interest (25, 30), because B lymphocytes are known to serve as efficient APCs for stimulating memory T cells and for priming naïve $CD4^+$ T cells (17). Therefore, the activation of B lymphocytes constitutes an important aspect of vaccine design.

BCRs have been shown to play important roles in the activation of B cells (24). This occurs by cross-linking of the BCRs for signal transduction, followed by the uptake of antigens and the accelerated expression of costimulatory molecules, leading to an enhanced immune response (23, 24). The Z domain has the ability to bind to a wide variety of Ig isotypes, including membrane-bound Ig (19). Thus, the IBDs bind to the B lymphocyte surface, and the tricomponent complex takes advantage of this unique feature. However, the utilization of a monomeric IBD may not activate B lymphocytes, because cross-linking of the BCRs does not occur in this situation. It may be possible, however, to cross-link the BCRs by using tandemly repeated multimers of IBDs (19). Agren et al. reported that tandem repeats of the D domain of SpA (DD)

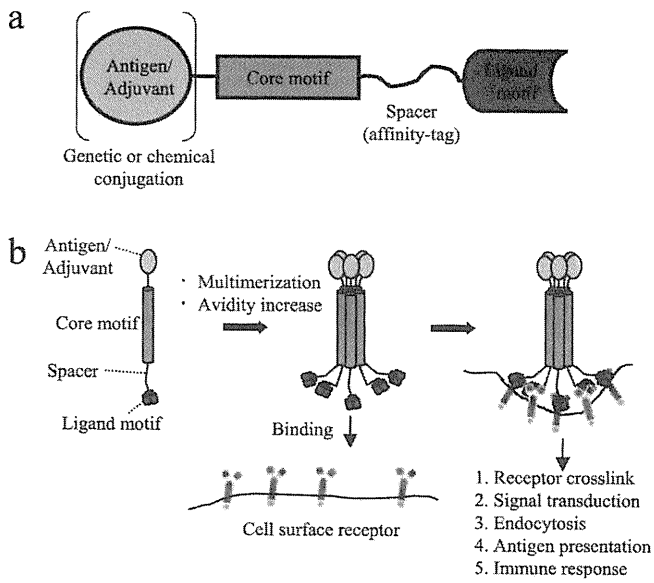

FIG. 10. Proposed mechanism of action of the tricomponent immunopotentiating system. (a) Design concept of the TIPS. Adjuvants or vaccine antigens, which may be proteins or other substances, are loaded onto the core motif by using genetic or chemical conjugation techniques. The core motif is connected to the ligand motif with a spacer arm, including an affinity tag. (b) Assembly of a monomeric tricomponent complex into a multimeric form, mediated by the coiled-coil core motifs, presumably increasing the avidity of the complex to facilitate the targeting of antigen-presenting cells mediated by the specific ligand motif used.

could be used to target and activate B lymphocytes (1). To test whether tandemly arranged IBDs exhibit an affinity for the IgG molecule equal to that of IBDs fused to the multimeric coiled-coil domains, we constructed the ZV delivery molecule and evaluated its binding affinity for human IgG. The dissociation constant (K_d) was determined according to a method described by Friguet et al. (13), and we found that the K_d values were 8.97×10^{-10} M and 1.56×10^{-9} M for the COMP-Z and ZV, respectively, suggesting that coiled-coil domain-mediated IBDs in a parallel arrangement have much higher avidity than multiple IBDs in a tandem arrangement with the same valence. Presumably as a consequence of this, the immunogenicity of the antigen loaded onto the COMP-Z became much higher than that of the antigen loaded onto the ZV as the delivery molecule (Fig. 7b). Besides the difference in their avidities for IgG, another explanation for the observation that the COMP-Z was more efficacious at inducing antibody responses to the loaded antigen than the ZV is that the COMP-Z, which contains multiple (i.e., 10) Cys residues per pentamer, could form cross-linked high-molecular-mass complexes when chemically coupled to antigens, whereas the ZV, which contains only 1 Cys residue, could not. Furthermore, the COMP-Z also exhibited immune-enhancing activity; when it was mixed with the antigen, it augmented serum IgG responses and vaccine efficacy (Fig. 4b and 6b and c).

B lymphocytes in the draining lymph nodes near the injection sites are presumed to be the *in vivo* target immune cells of the tricomponent complex. A large portion of the locally administered proteinaceous complex may move quickly through the afferent lymphatics into the follicles of the lymph nodes via

the subcapsular sinuses, where they first encounter repertoires of B lymphocyte clones (26). We hypothesized that in the follicles, the IBD-bearing complex binds to a larger number of B lymphocyte repertoires than do antigens lacking the IBD function, which would increase the chances of the loaded antigen encountering its cognate B lymphocytes. This may facilitate the uptake of loaded antigen by the cognate B lymphocytes and the presentation of this antigen to T lymphocytes, aiding in the transition of B lymphocytes to antibody-secreting cells after their move into the T lymphocyte area (6).

The TB and the COMP contain a multimeric coiled-coil domain (12, 20, 29) with self-assembling activity *in vivo* and *in vitro*. These domains have high thermal stability; the TB and COMP coiled-coil domains are resistant to 131°C and 100°C, respectively (15, 28). Thus, the core motifs composed of such domains may contribute to the overall molecular stability of the delivery molecules. In addition, they function as a scaffold for the vaccine antigen. This scaffold is potentially useful for the chemical coupling of various substances to the delivery molecules; these substances are not necessarily confined to proteinaceous materials but include, e.g., nonproteinaceous substances with innate immunity-inducing pathogen-associated molecular patterns (18). In this study, we selected a site-specific chemical conjugation scheme using the sulfhydryl group of the Cys residues within the core motifs to prevent masking of the ligand surface, which would likely interfere with binding to the receptors. According to our calculations, 5 mol of antigen was linked to 1 mol of the COMP-Z pentamer (data not shown). In addition, the core motifs also provided a convenient handle for affinity purification.

No significant differences in vaccine efficacy were detected between the tetravalent TB-based and pentavalent COMP-based tricomponent complexes. In addition, these two delivery molecules were produced with equal efficiency as secreted multimeric proteins from *E. coli*. The only distinctive difference between the two core motifs was that the former was exogenous and the latter was endogenous in mammals; thus, a relatively strong antibody response against the TB was raised in immunized mice, but almost no response against the COMP was observed (data not shown).

The genetic fusion method is generally superior to the chemical conjugation method for the construction of homogenous molecules; however, the efficiency of expression of soluble forms or of refolding, e.g., from *E. coli* inclusion bodies, can sometimes become problematic, depending on the type of antigen being fused to the delivery molecules. However, the production of all genetically conjugated tricomponent complexes is technically feasible, and we have already been successful in this approach with some other constructs (unpublished results). Besides the fact that both chemical and genetic fusion methods can be employed to construct the tricomponent complex, all three components can, in theory, be changed depending on the purpose. For example, any antigens, as we proved in part in this study, can be chemically loaded or genetically fused; different core motifs can be selected based on differences, for example, in their endogenous or exogenous origin or valence; other cell-targeting ligands, including other IBDs, can be employed (unpublished results); and DC-targeting motifs could also be integrated into the system in the future.

The results of the present study suggest that the tricomponent immunopotentiating system (TIPS) may become an efficacious antigen delivery system for the design of subunit vaccines against various infectious diseases (Fig. 10), where the use of weakly immunogenic recombinant proteins is desirable or unavoidable. TIPS, as a novel vaccine platform technology, therefore has the potential to be used in the development of various subunit vaccines against infectious diseases in the future.

ACKNOWLEDGMENTS

We thank Charles J. Arntzen of Arizona State University for valuable comments on our manuscript.

This work was supported by the following grants: Grants-in-Aid for Scientific Research (20590425) and Scientific Research on Priority Areas (21022034) from the Ministry of Education, Culture, Sports, Science and Technology, Japan; the Program for Promotion of Basic Research Activities for Innovative Biosciences from the Bio-oriented Technology Research Advancement Institution; the Cooperative Research Grant from the Institute of Tropical Medicine, Nagasaki University, Nagasaki, Japan; and a research grant from the Okinawa Industry Promotion Public Corp. (Naha, Okinawa, Japan).

REFERENCES

1. **Agren, L. C., L. Ekman, B. Lowenadler, and N. Y. Lycke.** 1997. Genetically engineered nontoxic vaccine adjuvant that combines B cell targeting with immunomodulation by cholera toxin A1 subunit. J. Immunol. **158:**3936–3946.
2. **Arakawa, T.** 2011. Adjuvants: no longer a 'dirty little secret', but essential key players in vaccines of the future. Expert Rev. Vaccines **10:**1–5.
3. **Arakawa, T., et al.** 2005. Nasal immunization with a malaria transmission-blocking vaccine candidate, Pfs25, induces complete protective immunity in mice against field isolates of *Plasmodium falciparum*. Infect. Immun. **73:**7375–7380.
4. **Arakawa, T., et al.** 2003. Serum antibodies induced by intranasal immunization of mice with *Plasmodium vivax* Pvs25 co-administered with cholera toxin completely block parasite transmission to mosquitoes. Vaccine **21:**3143–3148.
5. **Banchereau, J., and R. M. Steinman.** 1998. Dendritic cells and the control of immunity. Nature **392:**245–252.
6. **Batista, F. D., and N. E. Harwood.** 2009. The who, how and where of antigen presentation to B cells. Nat. Rev. Immunol. **9:**15–27.
7. **Burns, J. M., Jr., W. R. Majarian, J. F. Young, T. M. Daly, and C. A. Long.** 1989. A protective monoclonal antibody recognizes an epitope in the carboxyl-terminal cysteine-rich domain in the precursor of the major merozoite surface antigen of the rodent malarial parasite, *Plasmodium yoelii*. J. Immunol. **143:**2670–2676.
8. **Cella, M., F. Sallusto, and A. Lanzavecchia.** 1997. Origin, maturation and antigen presenting function of dendritic cells. Curr. Opin. Immunol. **9:**10–16.
9. **Cheng, P. C., M. L. Dykstra, R. N. Mitchell, and S. K. Pierce.** 1999. A role for lipid rafts in B cell antigen receptor signaling and antigen targeting. J. Exp. Med. **190:**1549–1560.
10. **Clark, M. R., D. Massenburg, M. Zhang, and K. Siemasko.** 2003. Molecular mechanisms of B cell antigen receptor trafficking. Ann. N. Y. Acad. Sci. **987:**26–37.
11. **De Gregorio, E., E. Tritto, and R. Rappuoli.** 2008. Alum adjuvanticity: unraveling a century old mystery. Eur. J. Immunol. **38:**2068–2071.
12. **Efimov, V. P., A. Lustig, and J. Engel.** 1994. The thrombospondin-like chains of cartilage oligomeric matrix protein are assembled by a five-stranded alpha-helical bundle between residues 20 and 83. FEBS Lett. **341:**54–58.
13. **Friguet, B., A. F. Chaffotte, L. Djavadi-Ohaniance, and M. E. Goldberg.** 1985. Measurements of the true affinity constant in solution of antigen-antibody complexes by enzyme-linked immunosorbent assay. J. Immunol. Methods **77:**305–319.
14. **Garcon, N., P. Chomez, and M. Van Mechelen.** 2007. GlaxoSmithKline adjuvant systems in vaccines: concepts, achievements and perspectives. Expert Rev. Vaccines **6:**723–739.
15. **Guo, Y., R. A. Kammerer, and J. Engel.** 2000. The unusually stable coiled-coil domain of COMP exhibits cold and heat denaturation in 4–6 M guanidinium chloride. Biophys. Chem. **85:**179–186.
16. **Hisaeda, H., W. E. Collins, A. Saul, and A. W. Stowers.** 2001. Antibodies to *Plasmodium vivax* transmission-blocking vaccine candidate antigens Pvs25 and Pvs28 do not show synergism. Vaccine **20:**763–770.
17. **Kakiuchi, T., R. W. Chesnut, and H. M. Grey.** 1983. B cells as antigen-presenting cells: the requirement for B cell activation. J. Immunol. **131:**109–114.

18. **Kawai, T., and S. Akira.** 2006. TLR signaling. Cell Death Differ. **13:**816–825.
19. **Ljungberg, U. K., et al.** 1993. The interaction between different domains of staphylococcal protein A and human polyclonal IgG, IgA, IgM and F(ab')2: separation of affinity from specificity. Mol. Immunol. **30:**1279–1285.
20. **Lupas, A. N., and M. Gruber.** 2005. The structure of alpha-helical coiled coils. Adv. Protein Chem. **70:**37–78.
21. **Miyata, T., et al.** 2011. Adenovirus-vectored *Plasmodium vivax* ookinete surface protein, Pvs25, as a potential transmission-blocking vaccine. Vaccine **29:**2720–2726.
22. **Miyata, T., et al.** 2010. *Plasmodium vivax* ookinete surface protein Pvs25 linked to cholera toxin B subunit induces potent transmission-blocking immunity by intranasal as well as subcutaneous immunization. Infect. Immun. **78:**3773–3782.
23. **Mond, J. J., E. Seghal, J. Kung, and F. D. Finkelman.** 1981. Increased expression of I-region-associated antigen (Ia) on B cells after cross-linking of surface immunoglobulin. J. Immunol. **127:**881–888.
24. **Monroe, J. G., and J. C. Cambier.** 1983. B cell activation. II. Receptor cross-linking by thymus-independent and thymus-dependent antigens induces a rapid decrease in the plasma membrane potential of antigen-binding B lymphocytes. J. Immunol. **131:**2641–2644.
25. **O'Hagan, D. T., and N. M. Valiante.** 2003. Recent advances in the discovery and delivery of vaccine adjuvants. Nat. Rev. Drug Discov. **2:**727–735.
26. **Pape, K. A., D. M. Catron, A. A. Itano, and M. K. Jenkins.** 2007. The humoral immune response is initiated in lymph nodes by B cells that acquire soluble antigen directly in the follicles. Immunity **26:**491–502.
27. **Peek, L. J., C. R. Middaugh, and C. Berkland.** 2008. Nanotechnology in vaccine delivery. Adv. Drug Deliv. Rev. **60:**915–928.
28. **Peters, J., W. Baumeister, and A. Lupas.** 1996. Hyperthermostable surface layer protein tetrabrachion from the archaebacterium *Staphylothermus marinus*: evidence for the presence of a right-handed coiled coil derived from the primary structure. J. Mol. Biol. **257:**1031–1041.
29. **Peters, J., et al.** 1995. Tetrabrachion: a filamentous archaebacterial surface protein assembly of unusual structure and extreme stability. J. Mol. Biol. **245:**385–401.
30. **Rodriguez-Pinto, D.** 2005. B cells as antigen presenting cells. Cell. Immunol. **238:**67–75.
31. **Saxena, A. K., et al.** 2006. The essential mosquito-stage P25 and P28 proteins from *Plasmodium* form tile-like triangular prisms. Nat. Struct. Mol. Biol. **13:**90–91.
32. **Saxena, A. K., Y. Wu, and D. N. Garboczi.** 2007. *Plasmodium* p25 and p28 surface proteins: potential transmission-blocking vaccines. Eukaryot. Cell **6:**1260–1265.
33. **Scandella, E., et al.** 2007. Dendritic cell-independent B cell activation during acute virus infection: a role for early CCR7-driven B-T helper cell collaboration. J. Immunol. **178:**1468–1476.
34. **Wang, L. D., and M. R. Clark.** 2003. B-cell antigen-receptor signalling in lymphocyte development. Immunology **110:**411–420.

Editor: J. H. Adams

Plenary paper

Accumulation of oxidative DNA damage restricts the self-renewal capacity of human hematopoietic stem cells

Takashi Yahata,[1,2] Tomomi Takanashi,[1] Yukari Muguruma,[1] Abd Aziz Ibrahim,[1,3] Hideyuki Matsuzawa,[1] Tomoko Uno,[1] Yin Sheng,[1] Makoto Onizuka,[3] Mamoru Ito,[4] Shunichi Kato,[2] and Kiyoshi Ando[1,3]

[1]Division of Hematopoiesis, Research Center for Regenerative Medicine, Tokai University School of Medicine, Isehara, Kanagawa, Japan; [2]Department of Cell Transplantation and Regenerative Medicine, Tokai University School of Medicine, Isehara, Kanagawa, Japan; [3]Department of Hematology, Tokai University School of Medicine, Isehara, Kanagawa, Japan; and [4]Central Institute for Experimental Animals, Kawasaki, Kanagawa, Japan

Stem cells of highly regenerative organs including blood are susceptible to endogenous DNA damage caused by both intrinsic and extrinsic stress. Response mechanisms to such stress equipped in hematopoietic stem cells (HSCs) are crucial in sustaining hematopoietic homeostasis but remain largely unknown. In this study, we demonstrate that serial transplantation of human HSCs into immunodeficient mice triggers replication stress that induces incremental elevation of intracellular reactive oxygen species (ROS) levels and the accumulation of persistent DNA damage within the human HSCs. This accumulation of DNA damage is also detected in HSCs of clinical HSC transplant patients and elderly individuals. A forced increase of intracellular levels of ROS by treatment with a glutathione synthetase inhibitor aggravates the extent of DNA damage, resulting in the functional impairment of HSCs in vivo. The oxidative DNA damage activates the expression of cell-cycle inhibitors in a HSC specific manner, leading to the premature senescence among HSCs, and ultimately to the loss of stem cell function. Importantly, treatment with an antioxidant can antagonize the oxidative DNA damage and eventual HSC dysfunction. The study reveals that ROS play a causative role for DNA damage and the regulation of ROS have a major influence on human HSC aging. (Blood. 2011;118(11):2941-2950)

Introduction

Maintenance of the hematopoietic system requires continual replenishment of mature blood cells from a rare population of bone marrow residing hematopoietic stem cells (HSCs). The alteration of the homeostatic control of hematopoiesis is considered to be a major culprit of drastic increase in pathologic incidences, such as bone marrow failure, anemia, and myeloid leukemia during aging.[1] However, the underlying mechanisms of pathogenesis of hematologic malignancy in elderly population remain poorly understood.

Mounting evidence supports the idea that the accumulation of somatic DNA damage is a main cause of aging in multicellular organisms.[2-5] Mice with mutations in various DNA repair genes exhibit accelerated aging in the hematopoietic system because of the premature exhaustion of HSCs, indicating that DNA repair is crucial for the maintenance of HSC self-renewal and hematopoietic function.[6,7] DNA damage can directly result from genotoxic treatment such as ionizing radiation (IR), or may simply occur as a consequence of genome duplication infidelity or of genotoxic effects of reactive oxygen species (ROS). ROS, such as superoxide anions and hydrogen peroxide, are byproducts of normal oxidative metabolism in eukaryotic cells and are involved in many signaling process. However, they can be harmful to cellular components, including DNA.[3,8,9] An uncontrolled elevation of intracellular ROS levels is believed to contribute to cellular aging and the senescence process.[3] In fact, an abnormal elevation of intracellular ROS levels has been implicated in the pathogenesis of various diseases, such as ataxia telangiectasia and Fanconi anemia.[3] In that sense, the maintenance of ROS levels, through highly regulated mechanisms, is essential for cellular homeostasis.[10]

Being continuously exposed to oxidants produced during metabolic activity and to external oxidants or oxidant-inducers through normal cellular physiology, DNAs within cells inevitably suffer the oxidative damage. Therefore, an accelerated proliferation of hematopoietic cells, which is expected to occur after clinical HSC transplantation, might lead to DNA damage through overexposure to oxidative stress generated on each cell cycle. Indeed, a hyperproliferation caused an accumulation of oxidative stress and resulted in functional exhaustion of murine HSCs, as shown by the failure to reconstitute hematopoiesis after serial transplantations.[11] Taken together, we hypothesize that the continuous production of ROS during long-term repopulation induces an accumulation of genomic damage that leads to exhaustion of human HSCs. We have previously developed a strategy that enables to examine the multipotency of a single human HSC using a reliable surrogate system.[12,13] By determining the in vivo repopulating dynamics of individual human HSCs, we demonstrated that the repopulating potential of the majority of human HSCs progressively deteriorated as they underwent extensive repopulation process. Furthermore, the self-renewing long-term repopulating clones stayed mainly in a quiescent state in the recipient bone marrow but expanded extensively on serial transplantation. It has not been clear, however, how the repopulating activity of human HSCs within the stem cell pool is regulated. In addition, functional influences of DNA damage response (DDR) pathway on the self-renewal capacity of human

Submitted January 10, 2011; accepted June 16, 2011. Prepublished online as *Blood* First Edition paper, July 6, 2011; DOI 10.1182/blood-2011-01-330050.

An Inside *Blood* analysis of this article appears at the front of this issue.

The online version of this article contains a data supplement.

The publication costs of this article were defrayed in part by page charge payment. Therefore, and solely to indicate this fact, this article is hereby marked "advertisement" in accordance with 18 USC section 1734.

HSCs remain unexplored. In this study, we address the effects of oxidative DNA damage during the lifespan of human HSCs.

Methods

Collection and fractionation of human CD34$^+$ cells

Cord blood (CB) and bone marrow samples were obtained after informed consent in accordance with the Declaration of Helsinki and with approval from the Tokai University Committee on Clinical Investigation. Bone marrow cells were collected from HSC transplant (HSCT) patients who were diagnosed as the complete remission. Information on HSCT patients is listed in supplemental Table 1 (available on the Blood Web site; see the Supplemental Materials link at the top of the online article). CD34$^+$ cell fraction was prepared using the CD34 Progenitor Cell Isolation Kit (Miltenyi Biotec). CD34$^+$-enriched cells were stained with allophycocyanin (APC)–conjugated anti-CD45 mAb (Coulter/Immunotech), and FITC-conjugated anti–lineage-specific antigens; CD2, CD3 (UCHT1), CD41 (P2), glycophorin A (11E4B-7-6), CD14 (MfP9), CD19 (SJ25C1), and CD56 (NCAM16.2; all from BD Biosciences), phycoerythrin (PE)–conjugated anti-CD38 (HB7; BD Biosciences), and PE–Texas Red (ECD)–conjugated anti-CD34 (581; Coulter/Immunotech) mAbs. Cells were gated on lineage marker negative and/or low expression region and Lin$^{-/low}$CD34$^+$ cells were fractionated according to their CD38 expression levels using the FACSVantage flow cytometer (BD Biosciences).

Cell cultures

Freshly isolated Lin$^-$CD34$^+$CD38$^-$ cells and Lin$^-$CD34$^+$CD38$^+$ cells were incubated with buthionine sulfoximine (BSO; 125μM) for 2 days in αMEM medium supplemented with TPO, SCF, and Flt3L (50 ng/mL each). To exclude the effect of external oxidants and reduce the ground level expression of γ-H2Ax foci, cells were cultured in hypoxic (5% O_2) conditions. For some experiments, N-acetyl-L-cysteine (NAC; 100μM, pH 7.0) was added to the culture media.

Human hematopoietic repopulation

NOD/Shi-scid, IL-2Rγc^{null} (NOG) mice[14] were obtained from the Central Institute for Experimental Animals and maintained in the animal facility of the Tokai University School of Medicine in microisolator cages. Mice were fed with autoclaved food and water. Nine- to 20-week-old NOG mice were irradiated with 220 cGy of X-rays. The following day, Lin$^-$CD34$^+$CD38$^-$ cells were injected into the retro-orbital plexus of the NOG mice. At the indicated times after transplantation, mice were humanely killed, and bone marrow cells were harvested. Human hematopoietic cells were distinguished from mouse cells by the expression of human CD45. Lin$^-$CD34$^+$CD38$^-$ cells isolated from pooled bone marrow cells of 3-5 recipient mice were used for the analyses. All experiments were approved by the animal care committee of Tokai University.

Serial transplantation

Bone marrow cells were obtained from recipient mice at 18 weeks after primary transplantation and injected intravenously into irradiated secondary or tertiary NOG recipients (2×10^7 cells per recipient). To examine the effect of antioxidant, mice were given feed containing 1.3% NAC for the entire repopulation period. CD34$^+$ cells were isolated from these mice, and serially transplanted into recipient mice (1×10^5 cells per recipient).

Detection of intracellular ROS

The intracellular ROS level was measured using a fluorescent probe 2′, 7′-dichlorofluorescene diacetate (DCF-DA). Cells were incubated with 10μM DCF-DA for 30 minutes, and the fluorescence was measured using a flow cytometor. The relative ROS level was calculated on the basis of the mean fluorescence intensity (MFI) of the DCF-DA and was presented as fold induction compared with the control group.

Cell-cycle analysis

Bromodeoxyuridine (BrdU) labeling was performed according to the manufacturer's instructions (BD Biosciences). For in vivo analysis, mice were injected with a single dose (1 mg) of BrdU. After 2 hours, Lin$^-$CD34$^+$CD38$^-$ cells were isolated, and BrdU incorporation was quantified by flow cytometry using the BrdU staining kit (BD Biosciences). For in vitro analysis, cells were pulsed with BrdU (10μM) for 30 minutes, and FACS analysis was performed.

Immunofluorescence micoscopy

Cells were seeded onto poly-L-lysine coated slides and fixed with ice-cold 70% ethanol for 15 minutes. After permeabilization with 0.2% Triton X-100 for 20 minutes, slides were treated with PBS containing 5% normal goat serum for 1 hour to block nonspecific binding of antibodies. Primary antibodies were applied overnight at 4°C. The following antibodies were used: γ-H2AX (JBW301; Millipore), ATM (Chemicon), 53BP1 (Cell Signaling Technology), CHK2 (Cell Signaling Technology), FOXO3a (Cell Signaling Technology), caspase-3 (Millipore), or p21^{CIP1} (12D1; Cell Signaling Technology). Cells were counterstained with DAPI. Images were captured with an LSM510 META confocal microscope (Carl Zeiss) and processed using Adobe Photoshop 7.0 (Adobe Systems). Fifty randomly captured images were used to quantify the foci formation.

Quantitative real-time PCR

RNA was isolated using the RNeasy micro kit (QIAGEN) and reverse transcribed. Each target cDNA was amplified on the same plate using the QuantiTect SYBR Green PCR Master Mix (QIAGEN) and the ABI Prism 7700 Sequence Detection System (Applied Biosystems). The sequence of PCR primers are: p16, 5′-GGGTCGGGTAGAGGAGGTG-3′ and 5′-GCCTCCGACCGTAACTATTCG-3′; p14, 5′-AGTGAGGGTTTTCGTG-GTTCA-3′ and 5′-TCCTCAGTAGCATCAGCACGAG-3′; p21, 5′-TGTCTTGTACCCTTGTGCCT-3′ and 5′-AATCTGTCATGCTGGTCTGC-3′; 18S rRNA, 5′-ACTCAACACGGGAAACCTCA-3′ and 5′-AACCAG-ACAAATCGCTCCAC-3′. The relative amounts of target genes were determined in reference to 18S rRNA. A comparative threshold cycle (C_T) was used to quantify transcripts. The value was calculated by the expression $2^{-\Delta\Delta CT}$. Each reaction was performed at triplicate.

Statistical analysis

Data were statistically analyzed using Prism 5.0 software (GraphPad Software). Results were analyzed by the 2-tailed unpaired Student t test after the evaluation of variants using the pooled datasets. The mean ± SD was presented in each graph. The numbers of γ-H2AX foci per cell were presented using box and whiskers graphs. P values $< .05$ were considered to be significant.

Results

Repopulating capacity of human HSCs deteriorate during long-term repopulation

A rare fraction of the Lineage$^-$(Lin$^-$)CD34$^+$CD38$^-$ cells represents repopulating human HSCs, a candidate human HSCs currently determined as severe immunodeficient mice hematopoietic repopulating cells (SRCs).[15] Previously, we demonstrated that quiescent human HSCs were maintained in the stem cell niche under steady-state conditions.[13] To examine the cell-cycle status of human HSCs during hematopoietic reconstitution after transplantation, recipient mice were administered with BrdU at several time points, and Lin$^-$CD34$^+$CD38$^-$ cells were analyzed for BrdU incorporation rate at 2 hours after the each administration. At 2 weeks after transplantation, Lin$^-$CD34$^+$CD38$^-$ cells exited G0/G1 and efficiently entered the S + G2/M phases of the cell

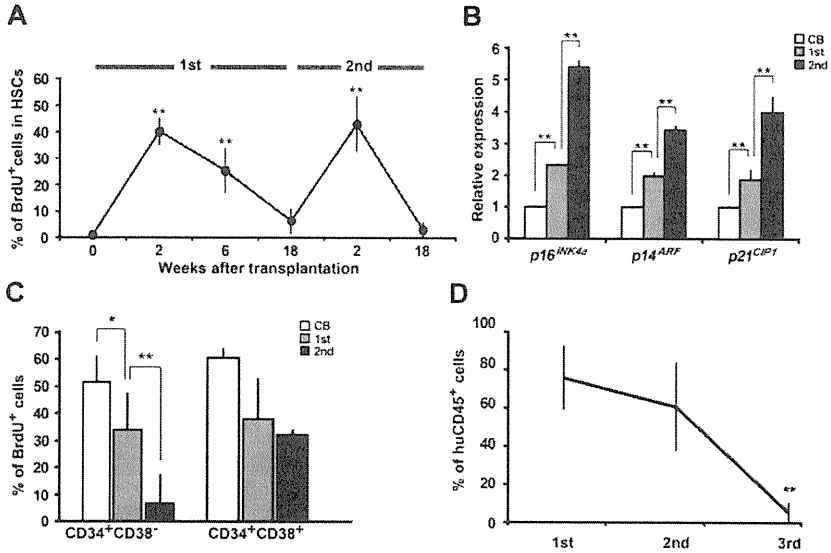

Figure 1. Functional assessment of long-term repopulating human HSCs. (A) Sublethally irradiated NOG mice were given transplants of CB Lin$^-$CD34$^+$CD38$^-$ cells. Recipient mice were administered with BrdU at the indicated time points (3 recipients in each time point), and Lin$^-$CD34$^+$CD38$^-$ cells were isolated at 2 hours after each administration. The BrdU incorporation rate for the isolated cells was analyzed by flow cytometry (**$P < .01$ relative to CB and 18 weeks after transplantation). (B) Relative expressions of *p16^{INK4a}*, *p14^{ARF}*, and *p21^{CIP1}* in Lin$^-$CD34$^+$CD38$^-$ cells were analyzed by quantitative real-time PCR. Each value was normalized to 18S rRNA expression and is presented as a fold induction compared with the levels detected in Lin$^-$CD34$^+$CD38$^-$ cells isolated from CB. Data were collected from 4 independent experiments (**$P < .01$). (C) Lin$^-$CD34$^+$CD38$^-$ cells and Lin$^-$CD34$^+$CD38$^+$ cells were obtained from CB and primary and secondary recipients' mouse bone marrow at 18 weeks after transplantation (3 recipients at the each time point). At 3 days after cultivation with cytokines, cells were pulsed with BrdU for 30 minutes, and then the BrdU incorporation rate was analyzed by flow cytometry (*$P < .05$, **$P < .01$). (D) Whole bone marrow cells obtained from each primary recipient mouse (n = 6) were serially transplanted into secondary (n = 6) and tertiary (n = 5) recipient mice. Human hematopoietic cell engraftment was assessed by the expression of human CD45 by flow cytometry at 18 weeks after each transplantation (**$P < .01$ relative to primary recipient).

cycle, suggesting the activation and expansion of human HSCs (Figure 1A). This cell-cycle transition was confirmed by the up-regulation of cyclin expressions (supplemental Figure 1). Interestingly, the proliferating Lin$^-$CD34$^+$CD38$^-$ cells regained quiescence at the later phase of transplantation. Lin$^-$CD34$^+$CD38$^-$ cells after secondary transplantation demonstrated the similar cell-cycle dynamics (Figure 1A). These results indicate that the cell-cycle status of human HSCs changes reversibly from quiescence to activation during repopulation.

To further investigate the quiescent status of HSCs at the different time points of the serial transplantation, we examined the expressions of cell-cycle inhibitors p16^{INK4a}, p14^{ARF}, and p21^{CIP1} in Lin$^-$CD34$^+$CD38$^-$ cells isolated from fresh CB and recipients' bone marrow at 18 weeks after primary and secondary transplantation. Serial transplantation resulted in marked up-regulation of cell-cycle inhibitors among the human HSC population (Figure 1B). In contrast, the expression levels of cell-cycle inhibitors in Lin$^-$CD34$^+$CD38$^+$ cells were unchanged throughout the same repopulation period (data not shown). Proliferation activity of human HSCs, determined as S-phase entry in response to cytokine stimulation, was assessed by BrdU incorporation in vitro. Although there were no significant changes in the percentage of BrdU incorporation among committed progenitors (Lin$^-$CD34$^+$CD38$^+$ cells), the proliferative capacity of human HSCs was reduced gradually during serial transplantation (Figure 1C). Consistent with these observations, the repopulating capacity of human HSCs in recipient mice was reduced drastically after the secondary transplantation (Figure 1D). These data suggest that self-renewal capacity of quiescent HSCs before and after transplantation is distinctly different even though they appear similar based on more than one criterion, that is, the cell-surface phenotype and cell-cycle status.

Decline of self-renewal potential of human HSCs is associated with an accumulation of DNA damage

Mice deficient in several genomic-maintenance pathways demonstrated a functional exhaustion of HSCs, because of an accumulation of genomic damage within HSC population.[6,7] To examine whether serial transplantation induces an accumulation of DNA damage in human HSCs, the number of γ-H2AX (γ-H2AX; pS139) foci, an indicator of the extent of DNA damage, was quantified in individual human cells recovered from recipient mice. The analysis revealed that whereas only an occasional γ-H2AX focus was observed in freshly isolated CB HSCs, the majority of Lin$^-$CD34$^+$CD38$^-$ cells isolated from serially transplanted mice exhibited multiple foci (Figure 2A). Furthermore, these cells exhibited cytologic evidence of activated DDR pathways, that is, up-regulation of DDR markers including ataxia telangiectasia mutated (ATM; pS1981), p53 binding protein (53BP1; pS1778), checkpoint kinase 2 (CHK2; pT68), and forkhead box O3a (FOXO3a; Figure 2B and quantitative data provided in supplemental Figure 2). Interestingly, no obvious accumulation of γ-H2AX foci was observed in committed progenitor cells (Lin$^-$CD34$^+$CD38$^+$) at any time of reconstitution (Figure 2A).

Hematopoietic repopulation stimulates the excessive production of ROS in HSCs

Being cell-intrinsic byproducts of normal metabolism, ROS can cause persistent DNA damage in any living cells and may contribute to cellular aging.[3,8] Therefore, we evaluated the ROS levels of reconstituting human HSCs at 18 weeks after transplantation. Lin$^-$CD34$^+$CD38$^-$ cells were isolated from serial transplant recipients, and the intracellular concentration of ROS was

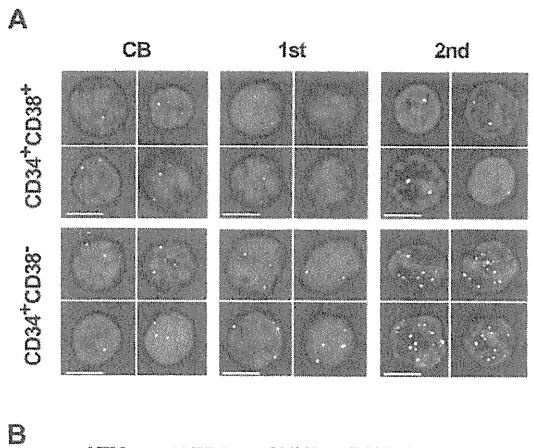

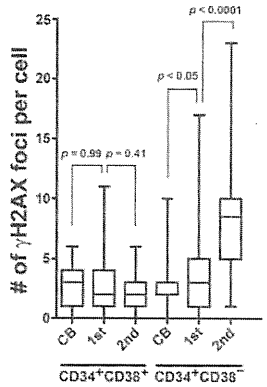

Figure 2. An accumulation of DNA damage in long-lived human HSCs. (A) Lin⁻CD34⁺CD38⁻ cells or Lin⁻CD34⁺CD38⁺ cells isolated from CB and recipient mice bone marrow at 18 weeks after primary (n = 10) and secondary (n = 15) transplantation were immunostained for γ-H2AX (γ-H2AX: green; DAPI: blue; left). All bars represent 5 μm. The box and whisker plot shows the number of γ-H2AX foci per cell. More than 50 cells in random fields on a slide were counted for 5 independent experiments. (B) Lin⁻CD34⁺CD38⁻ cells were immunostained with antibodies for ATM phosphorylated on Ser 1981 (green), 53BP1 phosphorylated on Ser 1778 (green), CHK2 phosphorylated on Thr 68 (green), or FOXO3a (green). DAPI (blue) was used to stain nucleus. All bars represent 5 μm.

determined by the intensity of DCF-DA staining using a flow cytometer. A gradual but marked increase in ROS levels was observed during serial transplantation (Figure 3A), reminiscent of the kinetics of DNA damage accumulation (Figure 2A-B). We also found that higher ROS levels were associated with increased DNA damage in human HSCs (Figure 3B). To investigate whether intracellular ROS levels influence the stem cell function, serial transplantations using ROS^{low} and ROS^{high} populations were performed. While ROS^{low} human HSCs retained the repopulation potential, the repopulating capacity of ROS^{high} human HSCs was almost diminished by the tertiary recipients (Figure 3B). These results suggest that a series of bone marrow reconstitution causes the elevation of intracellular ROS level and accumulation of DNA damage in human HSC, which lead to the reduction in stem cell function.

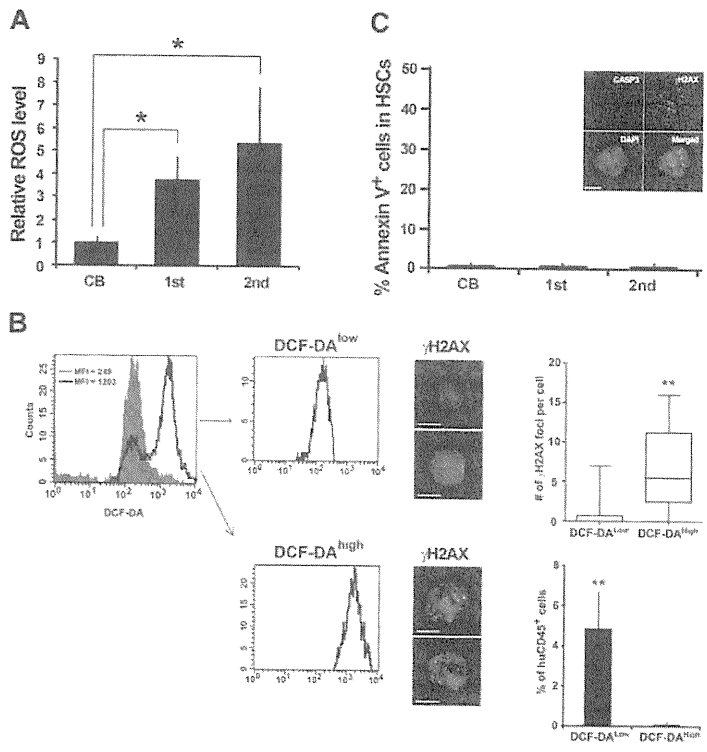

Figure 3. Increased ROS levels in long-lived human HSCs. (A) Lin⁻CD34⁺CD38⁻ cells were isolated from CB (n = 4) and recipient mouse bone marrow at 18 weeks after primary (n = 4) and secondary transplantation (n = 4). Intracellular ROS concentrations were determined by the intensity of DCF-DA staining using a flow cytometor. The relative ROS level is presented as a fold induction compared with the MFI value detected in Lin⁻CD34⁺CD38⁻ cells isolated from CB (*$P < .05$). (B) Representative sorting profiles of DCF-DA stained Lin⁻CD34⁺CD38⁻ cells isolated from secondary recipients' bone marrow cells. Gray shade indicates a DCF-DA–staining of Lin⁻CD34⁺CD38⁻ cells isolated from CB. Purified DCF-DA^{high} cells and DCF-DA^{low} cells were immunostained for γ-H2AX. The box and whisker plot shows the number of γ-H2AX foci per cell. More than 50 cells in random fields on a slide were counted for 3 independent experiments (**$P < .01$). Bars represent 5 μm. DCF-DA^{low} and DCF-DA^{high} Lin⁻CD34⁺CD38⁻ cells isolated from secondary recipient were transplanted into sublethally irradiated NOG mice. Twelve weeks after transplantation, engraftment levels of human hematopoietic cells were assessed by flow cytometry (3 recipients in each group; **$P < .01$). (C) Apoptosis in Lin⁻CD34⁺CD38⁻ cells was assessed by annexin V/PI staining (n = 3 in each group). Inserted images demonstrate the immunostaining results of Lin⁻CD34⁺CD38⁻ cells from secondary recipient. Positive staining for γ-H2AX (green) but not for active form caspase-3 (red) was detected.

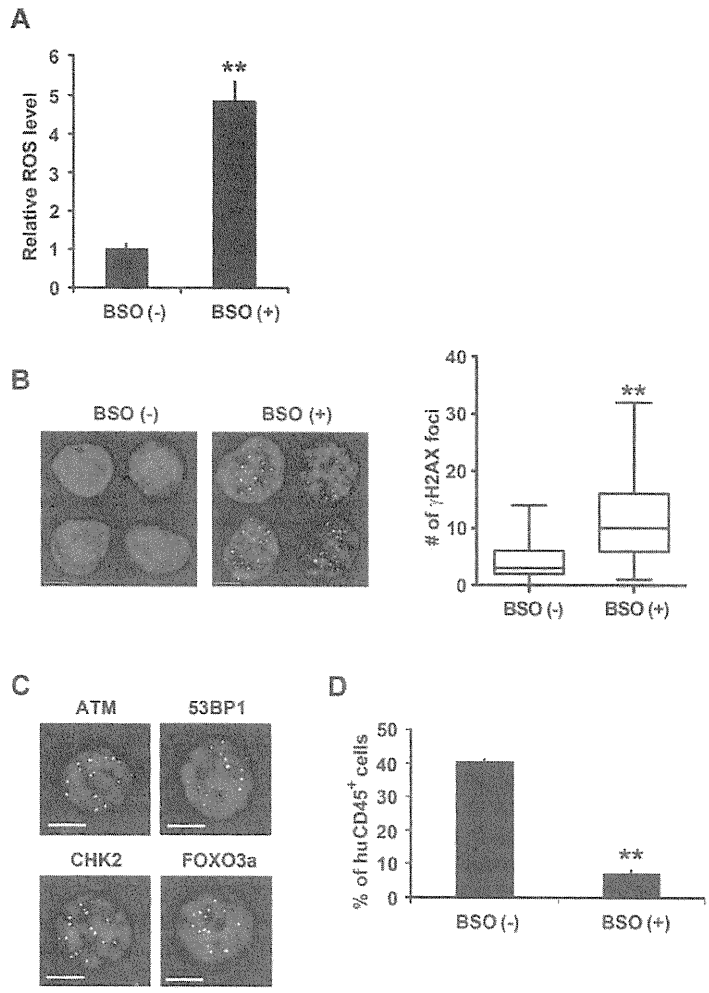

Figure 4. Oxidative DDR in human HSCs. (A) CB Lin$^-$CD34$^+$CD38$^-$ cells were cultured for 2 days with or without BSO. Intracellular ROS concentrations were determined by the intensity of DCF-DA staining using a flow cytometer. The relative ROS level is presented as a fold induction compared with the MFI value detected in Lin$^-$CD34$^+$CD38$^-$ cells cultured without BSO. Data were collected from 3 independent experiments (**$P < .01$). (B) CB Lin$^-$CD34$^+$CD38$^-$ cells cultured with or without BSO were immunostained for γ-H2AX (γ-H2AX: green; DAPI: blue). The number of γ-H2AX foci per cell is shown (right; **$P < .01$). Bars represent 5 μm. (C) CB Lin$^-$CD34$^+$CD38$^-$ cells treated with BSO were immunostained for ATM (p-S1981: green), 53BP1 (p-S1778: green), CHK2 (p-T68: green), and FOXO3a (green). All bars represent 5 μm. (D) BSO treated or nontreated CB Lin$^-$CD34$^+$CD38$^-$ cells were transplanted into NOG mice. Eight weeks after transplantation, engraftment levels of human hematopoietic cells were assessed by flow cytometry. Data were obtained from a total of 6 recipients in each group (3 independent experiments, **$P < .01$).

As a coping mechanism for internal and external cellular damage, the DDR machinery induces cell-cycle arrest in damaged cells. These cells may resume to cell-cycle progression once damage has been repaired, or cells that suffered irreparable DNA damage undergo apoptosis or permanent cell-cycle arrest.[3] We examined whether the DDR in human HSCs led to apoptotic cell death and found no evidence of apparent apoptotic cells among the long-lasting HSC population of primary and secondary transplants (Figure 3C). The results indicate that as a consequence of DDR, the long-lived HSCs may undergo senescence-like changes rather than apoptosis, or senescence-like cells may survive after damaged cells are cleared by apoptosis, either way leading to the persistence of DNA damaged foci in the stem cell compartment.

Oxidative DNA damage causes human HSC dysfunction

We then asked whether an increased ROS caused functional defects in the human HSC compartment. We added BSO, an inhibitor of glutathione synthetase, to the culture media to experimentally increase the intracellular ROS level of human HSCs (Figure 4A). To exclude the effect of external oxidants and to reduce the ground level expression of γ-H2AX foci, cells were cultured in a hypoxic (5% O_2) condition. BSO-treated cells and control cells were immunostained for γ-H2AX. The majority of the BSO-treated human HSCs presented multiple foci, contrasting to the control human HSCs in which only sporadic γ-H2AX foci were observed (Figure 4B). Further analyses revealed the cytologic evidence of activated DDR in BSO-treated human HSC cultures. The activated form of ATM, 53BP1, CHK2, and FOXO3a was detected (Figure 4C and quantitative data provided in supplemental Figure 3), thus demonstrating an activation of a series of DDR pathways initiated by the increased ROS levels in human HSCs. We therefore asked whether the oxidative DNA damage played a causative role in the functional defect in the human HSC compartment. The reconstitution activity of human HSCs was evaluated. As expected, the repopulating capacity of BSO-treated human HSCs was significantly reduced (Figure 4D). These data indicate that an accumulation of DNA damage in the HSC compartment initiated by the increased ROS level results in human HSC dysfunction.

It has been reported that the over-production of proinflammatory cytokines, such as IFN and TNF, is one element of the activation of the oxidative DNA damage checkpoint mechanisms in HSCs.[16,17] To address this issue, we examined whether the pro-inflammatory cytokines were involved in DNA damage observed in our human-to-mouse transplantation settings. First, we examined the production of murine and human TNF after transplantation in the hosts and found that the level of the cytokine was under

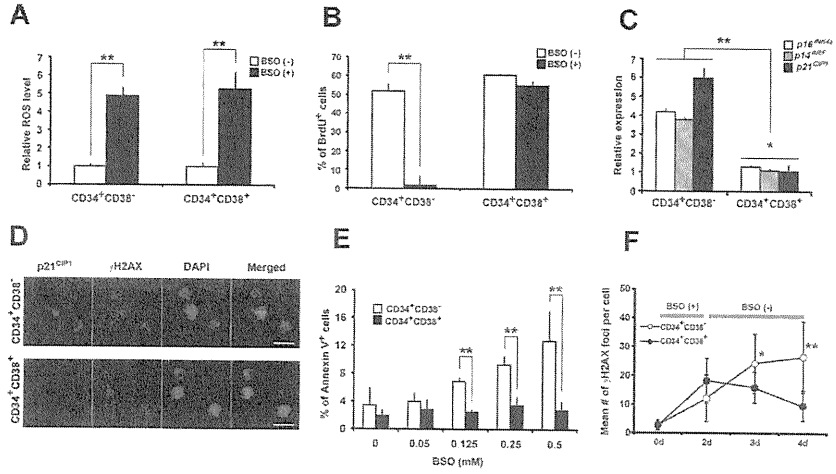

Figure 5. Distinctive response of human HSCs and progenitors to oxidative DNA damage. (A) CB Lin$^-$CD34$^+$CD38$^-$ cells and Lin$^-$CD34$^+$CD38$^+$ cells were cultured with or without BSO for 2 days. Intracellular ROS concentrations were determined by the intensity of DCF-DA staining using a flow cytometor. The relative ROS level is presented as a fold induction compared with the MFI value detected in cells cultured without BSO. Data from 2 independent experiments are shown (**$P < .01$). (B) Two days after BSO treatment, cells were pulsed with BrdU and analyzed by flow cytometry. Data from 2 independent experiments are shown (**$P < .01$). (C) Relative expressions of *p16^{INK4a}*, *p14^{ARF}*, and *p21^{CIP1}* in Lin$^-$CD34$^+$CD38$^-$ cells and Lin$^-$CD34$^+$CD38$^+$ cells cultured with or without BSO were analyzed at the end of 2-day culture by quantitative real-time PCR. Each value was normalized to 18S rRNA expression and is presented as a fold increase compared with the levels detected in cells cultured without BSO (**$P < .01$). (D) CB Lin$^-$CD34$^+$CD38$^-$ cells and Lin$^-$CD34$^+$CD38$^+$ cells cultured with BSO for 2 days were stained with γ-H2AX and p21^{CIP1} mAbs (γ-H2AX: green; p21^{CIP1}: red; DAPI: blue). Bars represent 5 μm. (E) At 2 days after BSO-treatment, the frequency of apoptotic cells was determined by annexin V/PI staining. Data from 3 independent experiments are shown (**$P < .01$). (F) The number of γ-H2AX foci per cell in Lin$^-$CD34$^+$CD38$^-$ cells and Lin$^-$CD34$^+$CD38$^+$ cells at the indicated time points. Cells cultured with BSO for 2 days were washed, replaced with fresh BSO-free media, and cultured for additional 1, 2, or 3 days (n = 4 in each time point; *$P < .05$, **$P < .01$, Lin$^-$CD34$^+$CD38$^-$ cells vs Lin$^-$CD34$^+$CD38$^+$ cells).

detection limit throughout the reconstitution period (supplemental Figure 4A). We then investigated the expressions of TNF and IFNγ in recipients' bone marrow cells and the effect of murine and human inflammation cytokines on the accumulation of DNA damage in human CB HSCs in vitro. Although the local production of murine TNF was slightly up-regulated (supplemental Figure 4B), the effect of this cytokine on DNA damage on human HSCs was negligible, given that no cross-reactivity of murine cytokines on human cells was confirmed (supplemental Figure 4C). Therefore, the effect of human proinflammatory cytokines appeared limited in our experimental model. We conclude that the DNA damages in human HSCs observed in our xenotransplantation settings are induced by a proinflammatory cytokine-independent manner. However, the proinflammatory cytokines may have a substantial influence on the stability of HSCs in the case of severe transplant-related diseases, such as GVHD or infection.

HSCs are predisposed for persistent DNA damage

Earlier in this study, we demonstrated that the extent of DNA damage in the Lin$^-$CD34$^+$CD38$^+$ progenitor cells was less prominent than in Lin$^-$CD34$^+$CD38$^-$ HSCs (Figure 2A). This may suggest the difference(s) in the response mechanism to oxidative DNA damage between HSCs and progenitors. To investigate this possibility, the biologic responses to oxidative DNA damage were compared between Lin$^-$CD34$^+$CD38$^-$ cells and Lin$^-$CD34$^+$CD38$^+$ cells. At day 2 of BSO treatment, no detectable difference was found in the induction of intracellular up-regulation of ROS levels (Figure 5A) or the number of γ-H2AX foci in the individual cells (Figure 5F) between HSCs and progenitor fractions. However, their biologic response to oxidative stress was quite different. The upsurge of intracellular ROS levels halted the cell cycle in HSCs almost completely (Figure 5B). This cell-cycle arrest of human HSCs in response to oxidative stress was further documented by the up-regulation of cell-cycle inhibitors p16^{INK4a}, p14^{ARF}, and p21^{CIP1} (Figure 5C). No such growth arrest (Figure 5B) or cell-cycle inhibitor up-regulation was observed in Lin$^-$CD34$^+$CD38$^+$ progenitor cells (Figure 5C). The oxidative DDR-induced cell-cycle inhibitor up-regulation in HSCs was confirmed by immunofluorescent microscopic analysis. Progenitor cells exhibited no apparent p21^{CIP1} expression (Figure 5D). We assessed the apoptotic response in these cells by annexin V/PI staining and found that a significantly higher percentage of cells underwent apoptosis in human HSC compartment than progenitor cells in vitro (Figure 5E). We then examined the kinetics of DNA lesions after BSO treatment. At the end of 2-day culture with BSO, cells were washed and continued to be cultured in BSO-free conditions for the indicated time period, and DDR was analyzed. The number of γ-H2AX foci per cell in Lin$^-$CD34$^+$CD38$^+$ cells declined comparatively faster than in Lin$^-$CD34$^+$CD38$^-$ cells (Figure 5F). We further examined the kinetics of DNA lesions after BSO treatment using Lin$^-$CD34$^+$CD38$^-$CD90$^+$CD45RA$^-$ cells, a more HSC-enriched population, and CD90$^-$CD45RA$^+$ multilymphoid progenitors (MLPs). The experiment resulted in the same outcome, confirming that the HSCs are predisposed for persistent DNA damage (supplemental Figure 5). These data indicate that HSCs are intrinsically more sensitive to the elevation of intracellular ROS levels than progenitors and explain why DNA lesions are less likely to be accumulated in progenitors in vivo (Figure 2A). The results support and clarify the interpretation for our earlier in vivo observation (Figure 3C) that the long-lasting HSCs are survivors of DNA damage that undergo senescence-like changes as a result of DDR.

Inhibition of ROS elevation rescues human HSCs from functional deterioration

We then asked whether the pharmacologic inhibition of intracellular ROS elevation could protect human HSCs from functional

degradation. Lin$^-$CD34$^+$CD38$^-$ cells were cultured with BSO and an antioxidant NAC. Treatment of human HSCs with the antioxidant prevented cells from the BSO-induced accumulation of DNA damage (Figure 6A) and apoptosis (Figure 6B). The pharmacologic inhibition of ROS elevation in the human HSC compartment also maintained the cytokine responding proliferation (Figure 6C) and repopulating activity (Figure 6D) of human HSCs.

We then attempted to rescue human HSCs from functional exhaustion during serial transplantation by treating recipients with the antioxidant. To minimize unavoidable superficial differences between treated recipients, recipients were transplanted with a limited number of cells. Recipients were fed with control or NAC-containing food during the entire reconstitution period starting immediately after the transplantation. The qualitative and quantitative changes in human HSC compartment were analyzed. Both the intracellular ROS level and the number of γ-H2AX foci were reduced in the human HSCs isolated from NAC-treated secondary recipients (Figure 6E-F). Consequently, the cytokine responsive proliferation (Figure 6G), the HSC compartment size (Figure 6H), and the self-renewal capacity of human HSCs (Figure 6I) were all maintained. Taken together, the results show that the elevated ROS level is the primary cause of DNA damage in human HSCs, and the pharmacologic inhibition of ROS elevation effectively prevents quantitative and qualitative deterioration of stem cell function in vitro and in vivo.

Accumulation of oxidative DNA damage is reproduced in the HSCs of elderly individuals and transplant recipients

We have shown so far that a repeated transplantation leads to functional decline among stem cell population. Thus, accumulated genomic damage in HSCs appears to be a physiologic indicator of stem cell aging. To test whether the DNA damage accumulation and subsequent stem cell dysfunction observed in the human-to-mouse xenotransplantation experiments is also applicable to human-to-human stem cell transplantation and normal human aging, we examined DNA lesions in Lin$^-$CD34$^+$CD38$^-$ cells and Lin$^-$CD34$^+$CD38$^+$ cells isolated from bone marrow of elderly healthy individuals and HSCT patients. Similar to the HSCs of the xenotransplantation experiments, the majority of the Lin$^-$CD34$^+$CD38$^-$ cells from elderly individuals (72-84 years; median: 79 years, n = 10) and HSCT recipients (34-56 years; median: 48 years, n = 8) exhibited multiple foci. Also consistent was no obvious accumulation of γ-H2AX foci in the Lin$^-$CD34$^+$CD38$^+$ progenitor cells (Figure 7A). Interestingly, the number of γ-H2AX foci of Lin$^-$CD34$^+$CD38$^-$ cells from middle-aged individuals (44-56 years; median: 50 years, n = 6) placed approximately in the middle of CB and aged samples. We compared the intracellular ROS level in the Lin$^-$CD34$^+$CD38$^-$ cells from each cell source. While elder HSCs exhibited higher ROS levels, although not statistically significant, than middle-aged HSCs (P = .068, Figure 7B), HSCs from transplant patients had a significantly higher level of intracellular ROS concentration than any other sources of HSCs (Figure 7B). This indicates that the HSC transplantation induces excessive production of ROS in the donor HSCs. We then investigated the repopulation activity of CD34$^+$ cells isolated from each group. As expected, human HSCs from aged individuals and HSCT recipients demonstrated deterioration in the repopulating capacity compared with CB samples (Figure 7C). Of note, HSCs from HSCT recipients exhibited a significantly higher number of γ-H2AX foci per cell and diminished repopulating activity compared with those of age-matched middle-aged individuals. These results indicate that DNA damage and

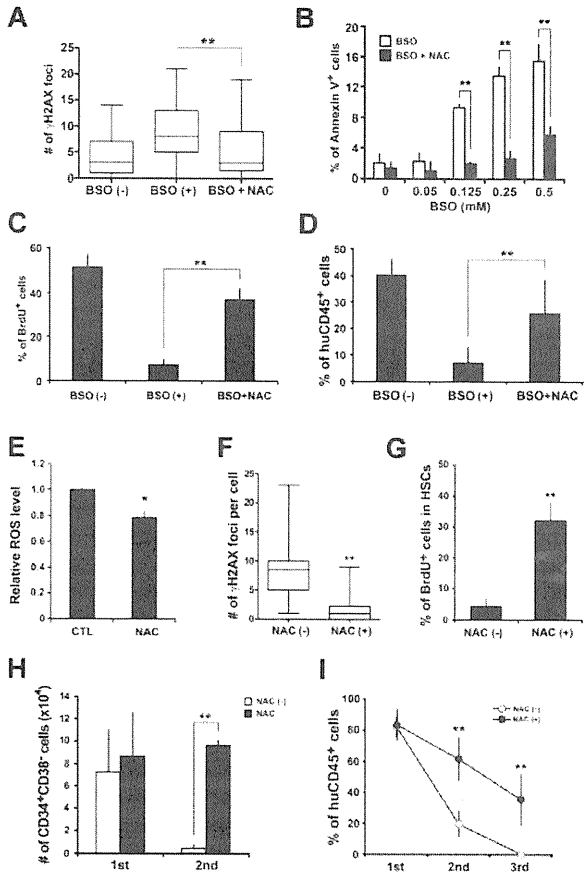

Figure 6. Antioxidant treatment prevents quantitative and qualitative loss of stem cell function in vitro and in vivo. (A) CB Lin$^-$CD34$^+$CD38$^-$ cells were cultured with BSO or BSO plus NAC and immunostained for γ-H2AX (γ-H2AX: green; DAPI: blue). The number of γ-H2AX foci per cell was obtained. The pooled data from 3 independent experiments are presented as the box and whisker plot (**$P < .01$ relative). (B) CB Lin$^-$CD34$^+$CD38$^-$ cells were cultured with BSO or BSO plus NAC for 2 days. The frequency of apoptotic cells was determined by annexin V/PI staining (n = 3 in each BSO concentration; **$P < .01$). (C) Cultured cells were pulsed with BrdU, and the BrdU incorporation was analyzed by flow cytometry (n = 4 in each culture condition; **$P < .01$). (D) Cells cultured under the indicated conditions were transplanted into NOG mice. Eight weeks after transplantation, engraftment levels of human hematopoietic cells were assessed by flow cytometry (6 recipients in each group; **$P < .01$). (E) Lin$^-$CD34$^+$CD38$^-$ cells were isolated from secondary recipients that had been fed with control or NAC-containing food, and intracellular ROS concentrations were determined by the intensity of DCF-DA staining using a flow cytometer. The relative ROS level is presented as a fold induction compared with the MFI value detected in Lin$^-$CD34$^+$CD38$^-$ cells isolated from control mice. Data were collected from 3 independent experiments (a total of 5 recipients in each group; *$P < .05$). (F) Lin$^-$CD34$^+$CD38$^-$ cells were isolated from secondary recipients that had been fed with control or NAC-containing food, and immunostained for γ-H2AX. The number of γ-H2AX foci per cell was counted. The pooled data from 3 independent experiments are presented as the box and whisker plot (9 recipients in each group; **$P < .01$). (G) Lin$^-$CD34$^+$CD38$^-$ cells isolated from NAC-treated or nontreated secondary recipients were cultured with cytokines for 3 days and then pulsed with BrdU. The percentage of BrdU positive cells was determined by flow cytometry. Data were collected from 3 independent experiments (a total of 9 recipients in each group; **$P < .01$). (H) The absolute number of Lin$^-$CD34$^+$CD38$^-$ cells in the recipient mice treated with or without NAC (5 recipients in each group; **$P < .01$). (I) Primary recipients were injected with 1×10^4 Lin$^-$CD34$^+$CD38$^-$ cells isolated from CB. Secondary and tertiary transplantation was performed at the 18th week of engraftment. A total of 1×10^5 CD34$^+$ cells pooled from 2-5 reconstituted recipients was transplanted into new groups of irradiated recipients. Engraftment levels of human hematopoietic cells were assessed by flow cytometry. Black circles indicate recipients that had been treated with NAC. White circles indicate nontreated recipients. Data were collected from 4 independent experiments (a total of 8 recipients in each group; **$P < .01$).

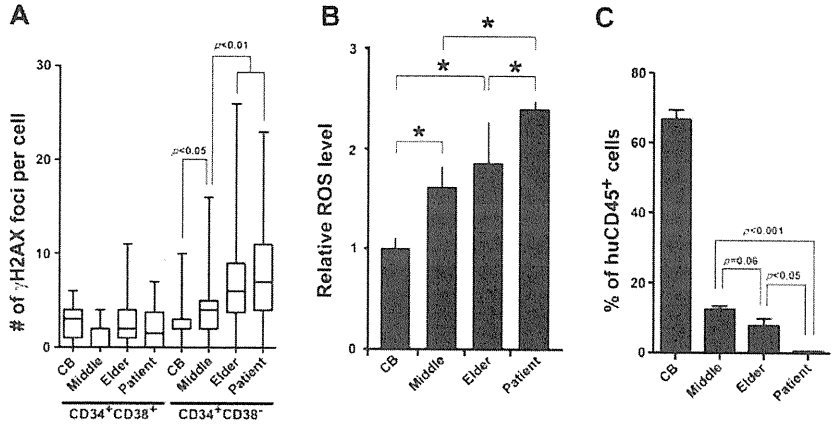

Figure 7. DDR in physiologic HSC aging. (A) Bone marrow Lin$^-$CD34$^+$CD38$^-$ cells isolated from middle-aged (n = 6) and elderly individuals (n = 10) as well as HSCT patients (n = 8) were immunostained for γ-H2AX. The number of γ-H2AX foci per cell for each subject is shown as the box and whisker plot. More than 50 cells in random fields on a slide were counted. (B) Lin$^-$CD34$^+$CD38$^-$ cells were isolated from HSCT patients and elderly individuals, and intracellular ROS concentrations were determined by the intensity of DCF-DA staining using a flow cytometer. The relative ROS level is presented as a fold induction compared with the MFI value detected in Lin$^-$CD34$^+$CD38$^-$ cells isolated from CB. Data were collected from 3 independent experiments (*$P < .05$). (C) Bone marrow CD34$^+$ cells (1×10^4 cells) isolated from middle-aged and elderly individuals and HSCT patients were transplanted into NOG mice. Eight weeks after transplantation, engraftment levels of human hematopoietic cells were assessed by flow cytometry (4 recipients in each group).

functional decline of human HSCs of transplant recipients and elderly individuals are indeed recapitulated in oxidative DDR-induced HSC dysfunction in our xenotransplantation experiments.

Discussion

DNA damage has been well accepted as a cause for cellular dysfunction and carcinogenesis.[2-5] In recent years, many theories have been proposed to explain the age-related functional decline of cells and tissues. One is the free-radical theory: the excess amounts of ROS, such as hydrogen peroxides, superoxides, and hydroxyl radicals, cause detrimental cellular damages that lead to premature aging.[3,10] ROS have previously been identified as a cause for the HSC defects in mice.[16,18-21] In mice lacking an oxidative stress responder, Atm or FoxO,[19-21] the HSC defect can be rescued by the addition of an antioxidant agent, thus indicating that the proper regulation of ROS level is indispensible for maintaining quiescent HSCs and sustaining hematopoiesis throughout the lifetime of an individual. The emerging question is whether ROS are responsible for the DNA damage leading to the HSC defect. Our study demonstrated that a regeneration-induced intracellular up-regulation of ROS resulted in the accumulated and persistent DNA lesions in human HSCs. In these HSCs, both ATM and FOXO3a, the oxidative stress responders also known to contribute to DDR pathways,[22,23] were activated. Importantly, the accumulation of DNA lesions was demonstrated in HSCs of HSCT patients and aged healthy individuals as well. The results of the inhibition of DNA damage accumulation with antioxidant treatment indicate that HSCs are highly sensitive to ROS elevation. The results also indicate that ROS play a causative role in DNA damage accumulation in human HSCs and have a major impact on stem cell aging.

A possible mechanism for the DDR observed in the human HSCs involves replication stress. Under steady-state conditions, the majority of human HSCs are maintained in a quiescent state, where they divide only infrequently, and at the same time, they produce proliferating progenitors that eventually give rise to mature hematopoietic cells and sustain blood homeostasis.[13,24,25] In this study, the transplanted HSCs had to undergo intensive proliferation to produce massive numbers of primitive progenitor cells to replace hematopoiesis in the myeloablated host environment. Such a forced stimulation of stem-cell proliferation is likely to create replication stress that involves ROS production and initiates DDR activation. The activation of DDR induces premature senescence in human HSCs, which results in the progressive loss of stem cell functions, in particular the capacity to self-renew. Such replication-induced DNA damage could occur in the normal aging process as well, and perhaps it plays a significant role in a variety of premature bone marrow failure syndromes or engraftment failure.

The accumulation of DNA damage during aging is a possible cause for the increased incidence of cancer in elderly populations.[6] In this study, long-lasting HSCs that underwent regenerative stress or normal aging process demonstrated persistent DNA damage without a significant increase in apoptotic cells. Long-lived HSCs that had escaped apoptosis demonstrated an accumulation of DNA lesions and the activation of cell-cycle inhibitors ($p16^{INK4a}$, $p14^{ARF}$, and $p21^{CIP1}$), an indication of senescence. Senescence could be characterized as a net accumulation of senescent cells in tissues or limitation of the regenerative potential within the stem cell pools, both of which may simultaneously contribute to aging of stem cells. The enormous functional demands and longevity of stem cells suggest that stem cells, particularly those from highly regenerative compartments, such as the skin and blood, are equipped with effective DDR mechanisms to ensure the genomic integrity over a lifetime. Induction of premature senescence in response to DNA damage under stress conditions could be one mechanism that protects stem cells from acquiring mutations that lead them to malignant transformation to putative leukemic stem cells. Progenitor cells play versatile functional roles to support the daily life of organisms, as opposed to stem cells, whose primary role is to provide and maintain the hematopoietic homeostasis. Our study showed that Lin$^-$CD34$^+$CD38$^+$ progenitor cells exhibited far fewer damaged lesions than HSCs, indicating efficient DNA repair mechanisms functioning in progenitor cells. Our findings are consistent with a notion that as a population the committed

progenitors are more resistant to DNA damage.[6,26,27] An alternative explanation is that during long-term repopulation, the frequency of damaged HSCs with higher ROS is increased gradually and markedly, and then only HSCs without oxidative DNA damage may successfully divide and contribute to the maintenance of hematopoietic homeostasis. As a result, those progenitor cells derived from lesser-damaged HSCs continue to have fewer damaged lesions.

In addition to our xenotransplantation model, ROS-induced accumulation of DNA damage was confirmed in human HSCs of HSCT patients and elderly individuals. Although the extent of DNA damage was similar in the 2 groups, HSCs from HSCT patients demonstrated far inferior ability to engraft in the murine host, suggesting that regenerating HSCs must have suffered much more stress than normal aging. This is consistent with an anecdotal clinical observation that hematopoietic recovery after chemotherapy takes longer in HSCT recipients. Successful outcome of clinical HSCT depends on several factors including the age of HSC donors. In a previous murine study, when a limited number of aged HSCs was transplanted into young recipients under competitive conditions, they showed an overall reduction in long-term repopulating potential, suggesting that aged HSCs are no longer able to meet the demand for blood production.[28] We showed that the ability to reconstitute hematopoiesis of murine host was significantly reduced in human HSCs from elderly individuals compared with HSCs from middle-aged individuals, indicating an age-related decline of stem cell function. Therefore, it seems relevant to set a limit at a certain age when selecting donors for clinical HSCT, not only because the physiologic stress for bone marrow collection may be unbearable for elderly donors but also because patients may not receive stem cells with optimal quality.

Regulatory mechanisms that ensure the maintenance of homeostasis and protection from tumorigenesis must be evolutionarily conserved in stem cells in highly regenerative tissues such as blood. To understand how stem cells cope with DNA damage caused by the endogenous and exogenous stress, much work has been invested on cell-intrinsic mechanisms in response to IR and revealed unique survival mechanisms furnished in stem cells.[26,27,29,30] In the present study, we focused on transplantation-induced DDR in clinical HSCT and aging-related DDR of human cells, which reflect a replication of stress under clinical procedures and physiologic cellular aging, respectively. Our study showed that a replication-induced intracellular elevation of ROS resulted in DNA damage in transplanted human HSCs and treatment with an antioxidant could antagonize the ROS-induced DNA damage and subsequent HSC dysfunction in a xenotransplantation model. Thus, the replication-induced DNA damage may offer a physiologic way of understanding the evolution of tumor from normal stem cells. Our findings would lead a new direction of optimization of HSCT condition and prevention of carcinogenesis.

Acknowledgments

The authors thank members of the Research Center for Regenerative Medicine of Tokai University for helpful discussion and assistance. They also thank members of the animal facility of Tokai University for meticulous care of the experimental animals; and members of the Tokai Cord Blood Bank for their assistance.

This work was supported by a Grant-in-Aid for Scientific Research from The Ministry of Education, Culture, Sports, Science and Technology of Japan (T.Y. and K.A.), and a Tokai University School of Medicine Project Research (T.Y.).

Authorship

Contribution: T.Y. conceived and designed the study, collected and assembled data, performed data analysis and interpretation, and wrote the manuscript; Y.M. wrote the manuscript; T.T., A.A.I., T.U., and Y.S. collected data; M.O., M.I., and S.K. provided study material; and K.A. conceived and designed the study and gave final approval of the manuscript.

Conflict-of-interest disclosure: The authors declare no competing financial interests.

Correspondence: Dr Kiyoashi Ando, Division of Hematopoiesis, Research Center for Regenerative Medicine, Tokai University School of Medicine, 143 Shimokasuya, Isehara, Kanagawa 259-1193, Japan; e-mail: andok@keyaki.cc.u-tokai.ac.jp.

References

1. Rossi DJ, Jamieson CH, Weissman IL. Stem cells and the pathways to aging and cancer. *Cell.* 2008; 132(4):681-696.
2. Garinis GA, van der Horst GT, Vijg J, Hoeijmakers JH. DNA damage and ageing: new-age ideas for an age-old problem. *Nat Cell Biol.* 2008;10(11):1241-1247.
3. Lombard DB, Chua KF, Mostoslavsky R, Franco S, Gostissa M, Alt FW. DNA repair, genome stability, and aging. *Cell.* 2005;120(4): 497-512.
4. Sharpless NE, DePinho RA. How stem cells age and why this makes us grow old. *Nat Rev Mol Cell Biol.* 2007;8(9):703-713.
5. Schumacher B, Garinis GA, Hoeijmakers JH. Age to survive: DNA damage and aging. *Trends Genet.* 2008;24(2):77-85.
6. Rossi DJ, Bryder D, Seita J, Nussenzweig A, Hoeijmakers J, Weissman IL. Deficiencies in DNA damage repair limit the function of haematopoietic stem cells with age. *Nature.* 2007; 447(7145):725-729.
7. Nijnik A, Woodbine L, Marchetti C, et al. DNA repair is limiting for haematopoietic stem cells during ageing. *Nature.* 2007;447(7145):686-690.
8. Barzilai A, Yamamoto K. DNA damage responses to oxidative stress. *DNA Repair (Amst).* 2004; 3(8-9):1109-1115.
9. Vilenchik MM, Knudson AG. Endogenous DNA double-strand breaks: production, fidelity of repair, and induction of cancer. *Proc Natl Acad Sci U S A.* 2003;100(22):12871-12876.
10. Beckman KB, Ames BN. The free radical theory of aging matures. *Physiol Rev.* 1998;78(2):547-581.
11. Ito K, Hirao A, Arai F, et al. Reactive oxygen species act through p38 MAPK to limit the lifespan of hematopoietic stem cells. *Nat Med.* 2006;12(4): 446-451.
12. Yahata T, Yumino S, Seng Y, et al. Clonal analysis of thymus-repopulating cells presents direct evidence for self-renewal division of human hematopoietic stem cells. *Blood.* 2006;108(7):2446-2454.
13. Yahata T, Muguruma Y, Yumino S, et al. Quiescent human hematopoietic stem cells in the bone marrow niches organize the hierarchical structure of hematopoiesis. *Stem Cells.* 2008;26(12):3228-3236.
14. Ito M, Hiramatsu H, Kobayashi K, et al. NOD/SCID/gamma(c)(null) mouse: an excellent recipient mouse model for engraftment of human cells. *Blood.* 2002;100(9):3175-3182.
15. Bhatia M, Wang JC, Kapp U, Bonnet D, Dick JE. Purification of primitive human hematopoietic cells capable of repopulating immune-deficient mice. *Proc Natl Acad Sci U S A.* 1997;94(10): 5320-5325.
16. Zhang X, Sejas DP, Qiu Y, Williams DA, Pang Q. Inflammatory ROS promote and cooperate with the Fanconi anemia mutation for hematopoietic senescence. *J Cell Sci.* 2007;120(9):1572-1583.
17. Baldridge MT, King KY, Goodell MA. Inflammatory signals regulate hematopoietic stem cells. *Trends Immunol.* 2011;32(2):57-65.
18. Jang YY, Sharkis SJ. A low level of reactive oxygen species selects for primitive hematopoietic stem cells that may reside in the low-oxygenic niche. *Blood.* 2007;110(8):3056-3063.
19. Ito K, Hirao A, Arai F, et al. Regulation of oxidative stress by ATM is required for self-renewal of haematopoietic stem cells. *Nature.* 2004; 431(7011):997-1002.
20. Tothova Z, Kollipara R, Huntly BJ, et al. FoxOs are critical mediators of hematopoietic stem cell